AEDC-TR-76-81

12 Ft

DIGITAL PHOTON CORRELATION DATA PROCESSING TECHNIQUES

SCIENCE APPLICATIONS, INC.
ATLANTA, GEORGIA 30339

July 1976

Final Report for Period May 3, 1974 – October 31, 1975

Prepared for

ARNOLD ENGINEERING DEVELOPMENT CENTER (DYR)
AIR FORCE SYSTEMS COMMAND
ARNOLD AIR FORCE STATION, TENNESSEE 37389

NOTICES

When U. S. Government drawings specifications, or other data are used for any purpose other than a definitely related Government procurement operation, the Government thereby incurs no responsibility nor any obligation whatsoever, and the fact that the Government may have formulated, furnished, or in any way supplied the said drawings, specifications, or other data, is not to be regarded by implication or otherwise, or in any manner licensing the holder or any other person or corporation, or conveying any rights or permission to manufacture, use, or sell any patented invention that may in any way be related thereto.

Qualified users may obtain copies of this report from the Defense Documentation Center.

References to named commercial products in this report are not to be considered in any sense as an endorsement of the product by the United States Air Force or the Government.

This final report was submitted by Science Applications, Inc., Atlanta, Georgia 30339, under contract F40600-74-C-0016 with the Arnold Engineering Development Center, Arnold Air Force Station, Tennessee 37389. Mr. Marshall K. Kingery (DYR) was the AEDC project monitor.

This report has been reviewed by the Information Office (OI) and is releasable to the National Technical Information Service (NTIS). At NTIS, it will be available to the general public, including foreign nations.

APPROVAL STATEMENT

This technical report has been reviewed and is approved for publication.

FOR THE COMMANDER

Marshall K Kingery

MARSHALL K. KINGERY
Research & Development
Division
Directorate of Technology

Robert O Dietz

ROBERT O. DIETZ
Director of Technology

UNCLASSIFIED

REPORT DOCUMENTATION PAGE		READ INSTRUCTIONS BEFORE COMPLETING FORM
1. REPORT NUMBER: AEDC-TR-76-81	2. GOVT ACCESSION NO.	3. RECIPIENT'S CATALOG NUMBER
4. TITLE (and Subtitle): DIGITAL PHOTON CORRELATION DATA PROCESSING TECHNIQUES.		5. TYPE OF REPORT & PERIOD COVERED: Final Report, 3 May 1974 - October 31 1975; 6. PERFORMING ORG. REPORT NUMBER
7. AUTHOR(s): W. T. Mayo, Jr.		8. CONTRACT OR GRANT NUMBER(s): F40600-74-C-0016 NEW
9. PERFORMING ORGANIZATION NAME AND ADDRESS: Science Applications, Inc. Atlanta, Georgia 30339		10. PROGRAM ELEMENT, PROJECT, TASK AREA & WORK UNIT NUMBERS: Program Element 65807F
11. CONTROLLING OFFICE NAME AND ADDRESS: Arnold Engineering Development Center(DYFS) Air Force Systems Command Arnold Air Force Station, Tennessee 37389		12. REPORT DATE: July 1976; 13. NUMBER OF PAGES: 131 (12) 135
14. MONITORING AGENCY NAME & ADDRESS(if different from Controlling Office)		15. SECURITY CLASS. (of this report): UNCLASSIFIED; 15a. DECLASSIFICATION DOWNGRADING SCHEDULE: N/A

16. DISTRIBUTION STATEMENT (of this Report)

Approved for public release; distribution unlimited.

17. DISTRIBUTION STATEMENT (of the abstract entered in Block 20, if different from Report)

18. SUPPLEMENTARY NOTES

Available in DDC

19. KEY WORDS (Continue on reverse side if necessary and identify by block number)

data processing
digital systems
photons
scattering
measurement
velocity
lasers

20. ABSTRACT (Continue on reverse side if necessary and identify by block number)

Presently available laser velocimeter (LV) electronic signal processing techniques are often inadequate for detection of light scattered by small scattering particles which are required for following the fluid motions. Example situations include low pressure and/or high velocity measurements. In other situations detection of larger scattering particles is difficult due to limited system sensitivity. Photon counting techniques offer improved system sensitivity by allowing velocity measurements to be made even when

DD FORM 1 JAN 73 1473 EDITION OF 1 NOV 65 IS OBSOLETE

UNCLASSIFIED

409327

20. ABSTRACT (Continued)
there are insufficient signal photons available to define the classical scattering signal. Such techniques are thus applicable when the presently used classical techniques are not.

The objective of this contract was the theoretical and experimental development of a new type of photon-counting processor for low-level dual-scatter LV signal detection. The contract was conducted in three separately funded phases: the first was a mathematical feasibility and preliminary hardware design study for a photon-counting processor; the second was a more detailed study of the statistical nature of low-level LV signals and their effects on low-level signal processing; and the third phase was the detailed design, construction, and demonstration of a new photon counting signal processor for photon resolved laser velocimeter signals. The effort under this contract has resulted in several significant conclusions both theoretical and experimental.

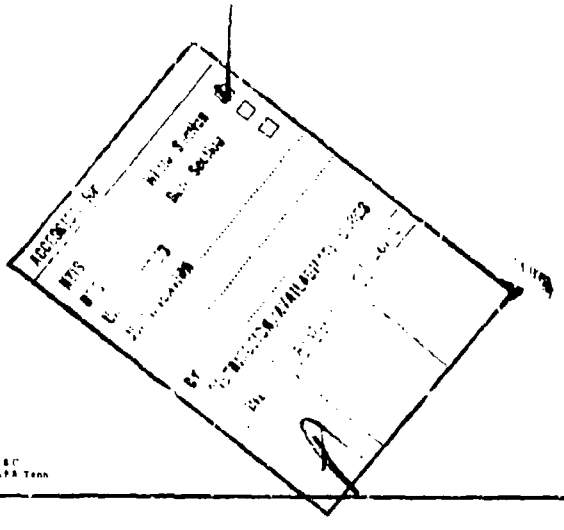

PREFACE

This technical report covers work performed under Contract No. F40600-74-C-0016 for the Arnold Engineering Development Center, Arnold Air Force Station, Tennessee. The work was performed between May 3, 1974 and October 31, 1975 by the Atlanta, Georgia Office of Science Applications, Inc. The program was under the direction of Captain M. L. Guiou, Arnold Engineering Development Center. The Program Element Number was 65807F.

The reproducibles used in the reproduction of this report were supplied by the author, W. T. Mayo, Jr., Science Applications, Inc.

SUMMARY

Presently available laser velocimeter (LV) electronic signal processing techniques are often inadequate for detection of light scattered by small scattering particles which are required for following the fluid motions. Example situations include low pressure and/or high velocity measurements. In other situations detection of larger scattering particles is difficult due to limited system sensitivity. Photon counting techniques offer improved system sensitivity by allowing velocity measurements to be made even when there are insufficient signal photons available to define the classical scattering signal. Such techniques are thus applicable when the presently used classical techniques are not.

The objective of this contract was the theoretical and experimental development of a new type of photon-counting processor for low-level dual-scatter LV signal detection. The contract was conducted in three separately funded phases: the first was a mathematical feasibility and preliminary hardware design study for a photon-counting processor; the second was a more detailed study of the statistical nature of low-level LV signals and their effects on low-level signal processing; and the third phase was the detailed design, construction, and demonstration of a new photon counting signal processor for photon resolved laser velocimeter signals. The effort under this contract has resulted in several significant conclusions both theoretical and experimental. These are summarized below.

Theoretical Poisson models have been formulated for dual-scatter LV signals with sufficient generality to include all signal regimes from classical signals with Gaussian noise down to photon-resolved signals which require photon counting techniques.

Analysis of conditional signal models has provided instantaneous signal-to-noise ratio and other statistical parameter equations not previously available in the LDV literature.

Analysis of Unconditional models has indicated the practical feasibility of improving detection sensitivity over burst-counter techniques by a factor between 100 and 1000 by using photon counting techniques.

A detailed analysis, including explicit mention of approximations required, of the expected value of direct photon correlation of LV signals from turbulent flow is provided. This both supports and points out limitations of previous results given by Pike and others.

A new Dual-Correlate-and-Subtract technique for new frequency measurement which utilizes only two delay values and one real-time high speed multiplier without clipping has been theoretically shown to be feasible. This feasibility is based on evaluation of the expectation for a system model to show convergence to mean frequency estimate, and on an rms variability analysis which indicates practical measurement times on the order of 0.5 seconds in transonic flow.

An electronically switchable, multipurpose, high-speed electronic signal processor with the potential speed for 10 sec time resolution and 10 nsec real time 4 bit multiplication has been designed and constructed using slow ECL integrated circuits on special-purpose 100 MHz wirewrap panel. The system implements the dual-correlate-and-subtract technique. It also has the potential of standard photon correlation without clipping by computer controlled scanning of the delays. The computer interface has not yet been constructed, however. If the computer interface is developed, the system will also be capable of measuring multipoint statistics of any high-speed events (up to 100 MHz).

Experimental measurements have been performed which verify the operation of the photon processor with 100 MHz input events and 40 MHz system clock operating speed. A sequential photon correlation of a low-level sinusoidally modulated optical source has been made with 25 nsec time resolution. The mean velocity of a low-speed jet was measured with the dual correlate of subtract mode under conditions for which no burst counter data could be obtained.

Photon counting experimental work requires much more care in selection and use of photomultiplier tube components than does burst-counter work. However, single photoelectron pulse height statistics and dynode collection efficiency can easily reduce the effective signal power to noise power ratio by a factor of 4 for two tubes with the same quantum efficiency. This can significantly effect a burst counter system sensitivity.

The statistical distribution of the amplitudes and rates of occurrence of classical bursts has been shown to be central in the problem of specifying or predicting the data rates and errors from any type of LV signal processor. Differential and cumulative rate/amplitude distributions have been formulated and analyzed theoretically and have been measured experimentally for an argon backscatter LV system. The results indicate that, for the data obtained, the smaller aerosols contribute more to the photon correlation accumulator than the larger ones. For the data measured, there would have been available less than 300 signals per second adequate in magnitude to produce burst counter data from scatterers larger than 0.7 micron in diameter while there would have been over 100,000 signals per second producing photon resolved signals from 0.2 - 0.3 micron diameter particles.

We have demonstrated both theoretically and experimentally that there are LV signals that require the use of photon counting techniques; and we have delivered a new type of

photon counting instrument which will potentially operate to 10 nsec time resolution with full 4 bit multiplication.

Further effort with computer controlled data collection is required to explore the potential of the new system and fully define its limitations.

CONTENTS

LIST OF ILLUSTRATIONS

LIST OF TABLES

1.0 INTRODUCTION

1.1 THE PROBLEM

Presently available laser velocimeter (LV) electronic signal processing techniques are often inadequate for detection of light scattered by small scattering particles which are required for following the fluid motions. Example situations include low pressure and/or high velocity measurements. In other situations detection of larger scattering particles is difficult due to limited system sensitivity. Photon counting techniques offer improved system sensitivity by allowing velocity measurements to be made even when there are insufficient signal photons available to define the classical scattering signal. Such techniques are thus applicable when the presently used classical techniques are not.

The objective of this contract was the theoretical and experimental development of a new type of photon-counting processor for low-level dual-scatter LV signal detection. The contract was conducted in three separately funded phases: the first was a mathematical feasibility and preliminary hardware design study for a photon-counting processor; the second was a more detailed study of the statistical nature of low-level LV signals and their effects on low-level signal processing; and the third phase was the detailed design, construction, and demonstration of a new photon counting signal processor for photon resolved laser velocimeter signals.

During the conduct of the contract a complementary theoretical effort with the NASA Langley Research Center was in progress (NAS1-13140 and follow-on NASA1-13737). The original feasibility mathematics developed in the first phase of this contract have been refined in the NASA effort. Portions of this report incorporate some of the NASA results for conciseness.

1.2 BACKGROUND

1.2.1 Signal Modeling

Earlier modeling efforts have treated LV signals for which the noise could be considered as additive independent, stationary, and Gaussian [1,2,3]. This is the limiting case of stationary Poisson shot noise which occurs for visible light photodetection when a steady light source such as a heterodyne reference beam [1] or high background light level [2] dominates the signal. In a recent simulation of low-level dual scatter signals, the accuracy of the noise model was extended by treating it as a nonstationary Gaussian process whose variance is proportional to the incident optical power.*

When we discuss "noise" in LV signal detection we are usually referring to the variation of the electronically detected signal with respect to a scaled version of the classical optical (power) signal incident on the PMT. In a general analysis the classical LV signals are also random processes due to the random amplitudes and the arrival times of the signal bursts. Mayo [1] has treated these signals as a Poisson process for steady flow, and Durrani [3] and George [5] have treated them for the turbulent flow case as Gaussian in the limit of high particle number density. A new book by Snyder [6] treats generalized Poisson processes in great detail. In particular he treats "doubly stochastic Poisson processes." These are inhomogeneous (nonstationary) Poisson processes for which the rate function is a random process. Such a description is appropriate either for the classical LV signal bursts with the random turbulent flow affecting the rate of burst occurrence or for the single photo-electron pulses from the PMT with the random classical bursts as the

*Modified version of noise model described in [4].

rate function. Clearly, when taken from the turbulence to the photo-electron pulses, a dual-scatter LV signal is a "triply stochastic" filtered Poisson process. This three level nature of the signals is illustrated by Figure 1.

1.2.2 Classical Detection Methods - Gaussian Signal Regime

Presently accepted burst-counter and frequency-tracker LV processors were developed by analogy with wide-band frequency modulation (FM) and radar receivers. For FM and radar applications frequency detection (zero-crossing) circuits generally require about 10 db signal power to noise power ratio within the bandwidth of the system filters. The signals in such cases are continuous and the noise is stationary and Gaussian. Comments by several speakers at the 1975 Minnesota LDA Symposium indicated that they had experimentally determined that their burst counter LV signal processors failed significantly when the signal power to noise power ratio (during a burst) was less than 10 db. The theory in this report shows that this 10 db condition occurs when there are approximately 10 photoelectron pulses per electronic response time τ_h. This response time is rise time or pulse width in the case of a low-pass filter. We have also defined this signal level as the lowest value of the "Gaussian" signal regime wherein the photomultiplier current can be modeled as the classical signal plus nonstationary Gaussian noise; (although neither Snyder [6] or Papoulis [7] give any helpful rules as to when this asymptotic approximation is valid). For lower signal power the signals must be treated as Poisson.

1.2.3 Photon Correlation Techniques - Very Low Level Signals

A radically different approach to LV signal detection was taken by Pike, Oliver, Jakeman, and others. Photon

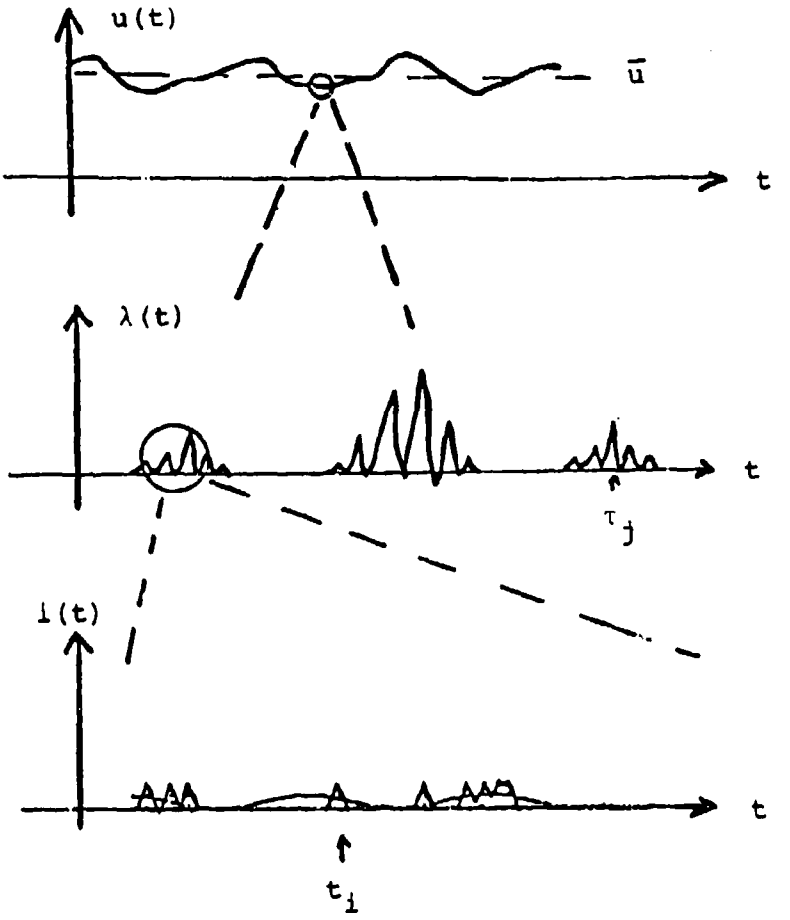

Figure 1. Triply Stochastic Nature of Low-Level LV signals: Turbulence, Bursts, and Photo electron Pulses.

counting techniques were developed for use with low-level photon resolved signals. The summary, results of several years of development of the single-clipping real-time Malvern photon correlator were described by Oliver and Jakeman in a recent book [8]. Dr. Pike described the application of photon-correlation to the processing of LV signals at the 1972 Purdue conference [9]. The presentation was apparently not received well by many American attendees and little has been done in the United States with the development of photon counting techniques until recently. Increased interest was shown by attendees of the 1974 Purdue conference.

One reason that the Malvern correlator has been slow to receive acceptance in this country is that the original theory for its use was based on the assumption of many scatters in the probe volume with the central limit theorem invoked to render the statistics of the scattered electric fields Gaussian. Since this assumption is known not to predominate in many applications of fringe-type LV's in unseeded air, none of the quoted theory for a single-clipping correlator is directly applicable. Other problems with the Malvern correlator for high-speed air flow besides its speed (minimum time resolution of 50 nsec) is the lack of any straightforward ways to extend the concept to the determination of flow time statistics such as correlations and power spectra.

1.3 SCOPE

In Section 2.0 of this report we introduce a three level Poisson signal model for dual scatter signals, define signal regimes, and provide instantaneous signal and noise equations valid for all signal levels. Section 3.0 describes the basic theory for photon correlation of LV signals, and defines and analyzes a photon counting frequency discrimination technique which we have called "Dual

correlate and subtract mode." Section 4.0 describes the design and the functional operation of a new high-speed experimental hardware system. Experiments which we have performed in the characterization of PMT's, in the measurement of burst amplitude distributions, and in the demonstration of feasibility of the new processor are all described in section 5.0. Sections 6.0 and 7.0 are devoted to Discussion and Conclusions; Appendix A provides a background information on Poisson processes. Appendix B is a brief report in itself which relates the burst amplitude/rate distributions to their optical sources and to the effects in photon counting and burst counter processors.

2.0 STATISTICAL THEORY OF DUAL SCATTER SIGNALS

2.1 POISSON MODELS

2.1.1 The Signal Current

The signal current from a photomultiplier tube (PMT) is modeled as inhomogeneous filtered Poisson random process (see Appendix A and reference 11) given by

$$i(t) = \sum_{-\infty}^{\infty} eg_i h(t - t_i) \tag{2.1}$$

where t_i = random time of occurrence of ith photoelectron
e = electronic charge
g_i = random charge gain of PMT multiplier
$h(t)$ = impulse response of PMT/filter system

The system response $h(t)$ is obtained as a convolution integral of the PMT impulse response $h_p(t)$, the transmission line impulse response $h_t(t)$, and the linear filter impulse response $h_f(t)$

$$h(t) = h_p(t) * h_t(t) * h_f(t) \tag{2.2}$$

where

$$f(t) * g(t) = \int_{-\infty}^{\infty} f(\alpha) g(t - \alpha) d\alpha \tag{2.3}$$

The superposition assumes operation in the linear range of the PMT electron multiplier. The use of the function $h_p(t)$ assumes that all single photo-electron pulses have the same shape except for amplitude. This neglects minor random shape variation.

The quantity which relates i(t) to the classical optical power is the statistical mean rate $\lambda(t)$ of occurrence of the randomly occurring photoelectron pulses. Thus

$$\lambda(t) = \frac{\eta P(t)}{h\nu} \tag{2.4}$$

where

η = product of cathode quantum efficiency and the dynode collection efficiency

$h\nu$ = Photon energy

$P(t)$ = Classical optical power, including background light and a constant component for dark current.

The effects of dark current are included by adding an equivalent power P_d. The model could be made more exact by adding a separate dark pulse summation with a separate distribution of amplitudes gd_i which are distributed somewhat differently than g_i; but this distinction will not often be required.

2.1.2 Superposition of Classical Single Burst Signals

The previous material includes little which restricts it to LV signals. We now consider the form of $\lambda(t)$ which is also treated as a filtered Poisson process.

Rigorous electromagnetic theory analysis of the scattered fields from more than one scatterer in the probe volume shows [12] mixing terms in P(t), the classical power incident on the PMT. However, in typical dual-scatter systems, the diffraction limited spot size of the collecting lens is much smaller than the probe volume; conservation of energy arguments show that in such cases the number of scatterers in the probe volume may be much greater than unity with statistically negligible coherent mixing, regardless

of the quality of the collecting lens [1]. This is significant even for LV systems which only trigger on isolated large signal bursts because we must also include in the model the effects of smaller scatterers which may exist at higher number density. We will take the position that at the PMT the classical power P(t) is the superposition of the background light power and the power from individual scatterers without coherent mixing cross terms. This will be acceptable so long as the average number of scatterers in one difrraction limited resolution cell of the receiver is less than unity, and there are no strong coherent reflections from windows or other optics.

A second consideration concerns the background light. Even when we neglect coherent mixing of signals, there are fluctuations in the classical background power. Bertolotti [13] provides a good review of these effects. Broadband background sources can be largely suppressed by the use of narrowband spatial and wave-length filters, but not always adequately enough for measurements from small scatterers. In such cases there are two considerations. If the background is modulated (for example fluorescent lights) the mean value signal is easily removed by electronic filters, but the non-stationary noise is not. When the broadband background is "steady" there are actually significant classical fluctuations at rates up to the optical bandwidth. However, Bertolotti shows that when the optical filter bandwidth is much greater than the PMT electronic bandwidth, the photoelectron statistics behave as though the classical fluctuations did not exist (they are averaged out). Laser light scattered from windows is not broadband and may exhibit undesirable fluctuations. This background should be minimized.

2.1.3 The Random Process $\lambda(t)$

With cognizance of the preceding discussion, we model $P(t)$ as the summation of a constant background P_b which includes broadband, laser, and dark current sources and an inhomogeneous filtered Poisson signal process.

$$\frac{h\nu\lambda(t)}{\eta} = P(t) = \left[\lambda_b + \sum_{j=-\infty}^{\infty} \lambda_j f(t - \tau_j, \bar{V}_j \bar{r}_j) \frac{h\nu}{\eta}\right] \quad (2.5)$$

where

τ_j = occurrence time of jth scatterer reaching $\bar{r}_j$ (2.6)
λ_j = random peak amplitude parameter
$\bar{V}_j$ = vector velocity of the jth scatterer
$\bar{r}_j$ = location of nearest approach of the scatterer trajectory to the center of the probe volume
$f(t,\bar{V},\bar{r})$ = normalized optical system response function

The notation in equation (2.5) explicitly shows that in general the shape of a burst (including signal period, signal envelope, and pedestal) is a function of the scatterer vector velocity and trajectory location. The response also has random λ_j amplitude which depends on both trajectory and particle scattering cross section. In general the set of instants τ_j are independent Poisson random events whose instantaneous rate, $R(t)$, is statistically correlated with the velocity vector.

2.1.4 Discussion of Model for the Classical Signal $\lambda(t)$

Equation (2.6) is cast in a general form which obscures certain details. First it assumes that the velocity of a scatterer remains constant while in the probe volume with a value $\bar{V}(\tau_j,\bar{r}_j)$. The extended theory of filtered Poisson

processes is sufficiently general to encompass the fact that the functional form of the optical response function $f(t,\bar{V},\bar{r})$ depends on two vector random variables.* However, Snyder [6] assumes that the vector random parameters are independent. We are not certain at the present time what the statistical dependence of the rate function $R(t)$ on the velocity $\bar{V}(t)$ may imply. We anticipate that in the future other work related to Snyder's book will be applied to equation (2.6) with less and less restrictive assumptions concerning the parameters.

2.2 CONDITIONAL SIGNAL STATISTICS

At times the models for the systems analysis problem may be simplified until analytical methods are applicable. In these cases the use of conditional statistics will usually simplify the analysis. Papoulis [7] discusses the use of conditional statistics at length. We illustrate this technique in an application of the theory in a later section. Basically for a multilevel random process the technique consists of assuming the higher level random processes are known and deterministic, evaluating conditional expectations assuming the higher level processes, then evaluating the expectation of the result with respect to the higher level processes. First we will consider statistics of $i(t)$ assuming the classical optical signal $\lambda(t)$ is known.

2.2.1 Instantaneous Mean, Variance, Autocovariance

The results in Appendix A may be applied to determine the instantaneous mean, variance and autocovariance of the

*Elementary shot noise theory is restricted to an impulse response function which is constant in shape.

signal. These are given in terms of the function $\lambda(t)$. The results are as follow:

$$m_i(t) = \langle i(t) \rangle = e\langle g_i \rangle \lambda(t) * h(t) \tag{2.7}$$

$$\sigma_i^2(t) = \langle (i(t) - \langle i(t) \rangle)^2 \rangle = e^2 \langle g_i^2 \rangle \lambda(t) * h^2(t) \tag{2.8}$$

$$C_{ii}(t_1, t_2) = \langle i(t_1) i(t_2) \rangle - \langle i(t_1) \rangle \langle i(t_2) \rangle \tag{2.9}$$

$$= e^2 \langle g_i^2 \rangle \int_{\infty}^{\infty} \lambda(\alpha) h(t_1 - \alpha) h(t_2 - \alpha) d\alpha$$

where $\langle\ \rangle$ denotes statistical expectation and where the asterisk again denotes the convolution integral. These results include the specification that $h_p(t)$, the impulse response of the PMT anode, have unit weight, i.e.,

$$\int_{-\infty}^{\infty} h_p(t) dt = 1 \tag{2.10}$$

in order to maintain conservation of charge. The functions $h_t(t)$ and $h_f(t)$ may include amplification or loss factors and need not have unity weight.

2.2.2 Conditional Noise and SNR

The concept of signal-to-noise ratio arose in communications theory when the "noise" was an additive stationary Gaussian random process totally characterized by a mean, mean-square deviation (variance), and a power spectral density. The ratio of the peak or average signal to the rms noise was a useful measure. The preceding equations show the mean-square deviation (variance) to be an instantaneous time function which is related to the classical signal.

Observation of real signals or computer simulations such as those shown in Figure 2 show that the concept of signal-to-noise-ratio is not an adequate figure of merit without careful specification.

As an example SNR definition, we consider a low-pass PMT impulse response as a rectangular function:

$$h(t) = \frac{1}{\tau_h} \text{ Rect } (t/\tau_h) \tag{2.11}$$

where

$$\text{Rect } (t) = 1, \quad |t| \leq 0.5 \tag{2.12}$$

$$= 0. \quad |t| > 0.5$$

If we now also assume that $\tau_n << T_o$ where T_o is the signal period of interest, then we could obtain an instantaneous SNR from equation 2.7 as

$$SNR(t) = m_i^2(t)/\sigma_i^2(t) = \langle g_i \rangle^2 \lambda^2(t)/\langle g_i^2 \rangle \lambda(t)/\tau_h \tag{2.13}$$

$$= \frac{\langle g_i \rangle^2}{\langle g_i^2 \rangle} \lambda(t)\tau_h$$

where the quantity $\langle g_i \rangle^2/\langle g_i^2 \rangle$ is typically between 0.5* and 1.0 with magnitude depending on the relative variance of the PMT single photoelectron pulse gain. For an ideal tube the quantity $\lambda(t)\tau_h$ would be the instantaneous SNR. This is not so useful since it's a time function instead of a number.

As an alternative, we may take the local time average of the SNR given by (2.13) over a signal cycle near the peak of the pedastal. This would give

---

*The RCA PMT Manual indicates typical decrease in rms SNR is [14] greater than 0.707. This is equivalent to 0.5 in mean square ratio.

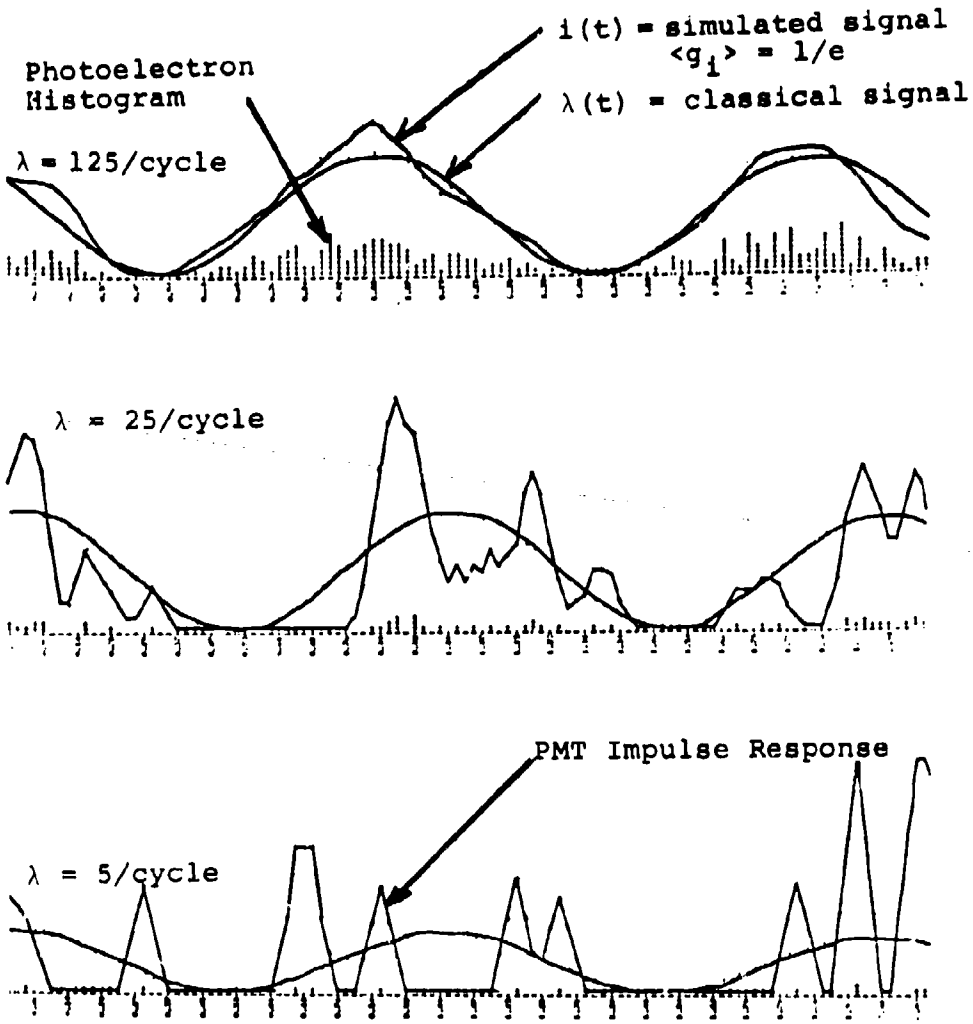

Figure 2. Digital Simulations of the Central Portions of Gaussian, Photon-Limited, and Photon-Resolved LV Signal Bursts.

$$SNR_{AVpeak} \approx \lambda_j \tau_h \qquad (2.14)$$

where λ_j is the peak value of the pedastal of the jth signal burst, if we assume sparse non-overlapping bursts. We observe that equations (2.7) through (2.9) are valid when h(t) is a bandpass function, but (2.14) is then meaningless unless we redefine τ_h for a bandpass h(t). Also we note that this definition would be necessary for meaningful use with a burst-counter processor, since it is the bandpass filtered AC signal to wide-band noise power that is significant in that case. We leave the subject of SNR with the advice that one obtain a careful definition before comparing notes with others.

2.2.3 Signal Regimes

The idealized quantity $SNR_{av\,peak}$ given in equation (2.14) as $\lambda_j \tau_h$ is at least a useful quantity in defining a classification system of signal regimes for a low-pass filtered signal. The following definitions of a photon-resolved, a photon-limited, and a Gaussian signal regime have been somewhat arbitrarily* identified:

The signal is photon resolved if $\lambda\tau_h << 1$. In this case the probability of two or more photoelectron events occurring within the response time τ_h is small. Its appearance is that of individual pulses which vary in height due to the randomness of g_i. Photon counting methods are appropriate. The conditional mean value of i(t) is still proportional to $\lambda(t)$. This condition is illustrated by the lower trace in Figure 2.

For $\lambda\tau_h >> 1$, the signal i(t) is asymptotically a

*See Papoulis [7] page 571. No specific limit on the magnitude of $\lambda\tau_h$ is given. We define the photon limited regime as $0.1 < \lambda\tau_h < 10$.

non-stationary Gaussian Process.* In this case the first and higher order probability density functions for i(t) at any set of instants $(t_1, t_2, \ldots)$ may be determined immediately by plugging the mean, variance and auto-covariance from the preceding equations into well known Gaussian formulas. Under these same conditions the signal display appears to the eye as a classical signal $m_i(t)$ plus Gaussian noise. This condition is illustrated by the upper trace in Figure 2. The major difference between this case and that of classical communications theory problems is that the σ value for the noise is signal (time) and system dependent. Usually, signals in the Gaussian regime are suitable for processing by classical methods (burst counter and/or tracker).

The photon limited regime is that for which $\lambda\tau_h$ is within an order of magnitude of unity. No mathematical simplifications are possible. Visually the signal appears as shown in the middle trace of Figure 2. The upper limits of photon counting techniques and the lower limits of conventional techniques both fall in this range.

2.3 UNCONDITIONAL STATISTICS

2.3.1 Long Time Mean, Variance, Autocovariance

Equations 2.7 - 2.9 include the assumed deterministic classical signal λ(t) which is proportional to instantaneous optical power. When we wish later to evaluate the long-time average result which accumulates during a photon counting

*See Papoulis [7] page 571.

experiment, it will be necessary to treat $\lambda(t)$ as an ergodic random process with long-time-average equal to the unconditioned statistical mean:

$$\langle\lambda(t)\rangle = \lambda$$

We also make use of the autocorrelation of $\lambda(t)$:

$$\langle\lambda(t)\lambda(t+\tau)\rangle = R_\lambda(\tau) \tag{2.15}$$

Now from equation 2.7 taking the expectation with respect to $\lambda(t)$ gives the mean current as

$$\langle i\rangle = e\langle g_i\rangle\langle\lambda\rangle \int_{-\infty}^{\infty} h(t)dt \tag{2.16}$$

where the integral is unity unless $h(t)$ includes preamplification or attenuation external to the PMT. In order to determine the long time variance σ_i^2 we do not get the correct answer by taking the expectation of $\sigma_i^2(t)$ given by equation 2.8. Rather, one determines the conditional value of $\langle i^2(t)\rangle$ by adding the square of 2.7 to 2.8. The expectation with respect to $\lambda(t)$ follows; finally, the square of equation 2.16 is subtracted from the unconditional expectation of $i^2(t)$. When all these steps are completed, and similar ones for the unconditional autocovariance, we obtain:

$$\sigma_i^2 = e^2[\langle g_i\rangle^2 \int_{-\infty}^{\infty} R_\lambda(\alpha) f_h(\alpha)d\alpha + \langle g_i^2\rangle \int_{-\infty}^{\infty} h^2(\alpha)d\alpha \tag{2.17}$$

$$- \langle g_i\rangle^2\langle\lambda\rangle^2 \left(\int_{-\infty}^{\infty} h(\alpha)d\alpha\right)^2]$$

$$C_{ii}(\tau) = e^2[\langle g_i\rangle^2 R_\lambda(\tau) * f_h(\tau) + \langle g_i^2\rangle\langle\lambda\rangle f_h(\tau) \tag{2.18}$$

$$- \langle g_i\rangle^2\langle\lambda\rangle^2 \left(\int_{\infty}^{\infty} h(\alpha)d\alpha\right)^2]$$

where

$$f_h(\tau) = \int_{\infty}^{\infty} h(\alpha)h(\alpha+\tau)d\alpha \qquad (2.19)$$

The second term in the expression for $C_{ii}(\tau)$ vanishes for τ greater than the impulse response time for the PMT and filter combination; the last term is the square of the mean; the first term is the correlation of $\lambda(t)$ smoothed by the correlation of $h(t)$ with itself.

2.3.2 Ideal Photon Correlation

An idealized photon correlator counts all photoelectron emission events during successive uniformly spaced clock periods of duration $\Delta\tau$. The number sequence $\{n_k\}$ which results is algebraically manipulated to yield the summation of terms $n_k n_{k+p}$. In evaluating the expected value of the result of accumulating such a sum we encounter the need to evaluate the quantities $\langle n_k \rangle$ and $\langle n_k + n_{k+p} \rangle$. These expectations may be evaluated using equations 2.16 - 2.19 by assuming

$$h(t) = \text{Rect}(t/\Delta\tau) \qquad (2.20)$$

$$g_i = 1/e$$

where Rect(t) was defined in equation 2.12 and

$$\int h(t)dt = \Delta\tau \qquad (2.21)$$

With these assumptions, i(t) is equal to the number of photo-electron events in the interval $(t - \Delta\tau/2,\ t + \Delta\tau/2)$ and the formulas reduce to

$$\langle i \rangle = \langle n_k \rangle = \langle \lambda \rangle \Delta\tau \qquad (2.22)$$

$$\text{var } n_k = \sigma_i^2 = \langle n_k^2 \rangle - \langle n_k \rangle^2 = \Delta\tau \int_{-\infty}^{\infty} R_\lambda(\alpha)\ \Lambda\left(\frac{\alpha}{\Delta\tau}\right) d\alpha \quad (2.23)$$

$$+ \langle\lambda\rangle\Delta\tau - \langle\lambda\rangle^2\Delta\tau^2$$

$$\langle n_k n_{k+p} \rangle = C_{ii}(p\Delta\tau) + \langle i \rangle^2 \quad (2.24)$$

$$= \Delta\tau R_\lambda(\tau) * \Lambda(\tau/\Delta\tau)\big|_{\tau = p\Delta\tau,\, p \neq 0}$$

where the correlation integral of equation 2.19 produces a triangular function, i.e.

$$\int \text{Rect}\left(\frac{\alpha}{\Delta\tau}\right)\ \text{Rect}\left(\frac{\alpha+\tau}{\Delta\tau}\right) d\alpha = \Delta\tau\Lambda(\tau/\Delta\tau) \quad (2.25)$$

where

$$\Lambda(\tau/\Delta\tau) = 1 - |\tau|/\Delta\tau \qquad |\tau| \leq \Delta\tau \quad (2.26)$$

$$= 0 \qquad |\tau| > \Delta\tau$$

When $\Delta\tau$ is much smaller than a characteristic signal period, then the last two formulas simplify:

$$\langle n_k n_{k+p} \rangle = \Delta\tau^2\ R_\lambda(p\Delta\tau),\ p \neq 0 \quad (2.27)$$

$$= \Delta\tau^2\ R_\lambda(0) + \langle\lambda\rangle\Delta\tau,\ p = 0$$

$$\text{var } n_k = \sigma_i^2 = \langle\lambda\Delta\tau\rangle + \Delta\tau^2\ (\langle\lambda^2\rangle - \langle\lambda\rangle^2) \quad (2.28)$$

i.e.,

$$\text{var } n_k = \langle n_k \rangle + \Delta\tau^2\ \text{var } \lambda \quad (2.29)$$

We observe that the generally accepted result that the photon correlation is shaped like the correlation of the classical signal is true subject to the jump discontinuity at zero delay and subject to the triangular weighting function which behaves as a low-pass filter with respect to the details of $R_\lambda(\tau)$.

2.4 AMPLITUDE/RATE STATISTICS FOR CLASSICAL BURST SIGNALS

The statistical distribution of the classical burst amplitudes and the rate of occurrence versus amplitude are very significant in the characterization of any LV signal processor. It is generally accepted, for example, that the optimum rate of occurrence of bursts for a burst counter is less than the inverse burst duration (non-overlapping bursts.) It is also generally known that the error check circuits cause a burst counter to emphasize larger amplitude (good signal to noise ratio) signals. On the other hand, a photon counting processor must emphasize the lower amplitude signals in a distribution; the higher amplitude signals would produce only a single threshold crossing and otherwise be neglected by the system. It is therefore not possible to compare two different types of signal processors without knowing the signal amplitude distributions and the processor behavior as a function of burst amplitude and other factors. Finally, in order to relate processor behavior to a specified particle size distribution, one must first relate the particle size distribution to the burst amplitude distributions and then do all the other things already discussed.

During the initial phases of this contract we formulated analytical models and defined amplitude/rate functions. This task proved to be more complicated than we would have imagined. The results we obtained during that portion of

the study are not general in nature and need additional refinement for improved conciseness and clarity. However, the subject matter is significant for future LV application improvements, so we have included the material from our earlier interim report as Appendix B.

3.0 CONCEPTUAL FEASIBILITY OF A NEW LV SIGNAL PROCESSOR

In this section we postulate a new type of photon-counting LV signal processor and present a feasibility analysis which describes the basic principles. We begin by using the theory of Section 2.0 to derive the expected result for an ideal photon correlator. This theory is then extended to the Dual-Correlate-and-Subtract-Technique which we have proposed.

3.1 SIGNAL MODELS FOR $R_\lambda(\tau)$

The form of equation 2.5 is quite general. In most practical systems, the function $f(t,\bar{V}_j,\bar{r}_j)$ which describes the optical response with respect to particle position and velocity is complicated when the effects of limiting pinhole apertures are included. For the present we assume a simplified low turbulence model which assumes a burst with perfect contrast and constant shape:

$$\lambda(t) = \lambda_b + \sum \lambda_j f(t - \tau_j)[1 + \cos\ \omega_j(t - \tau_j)] \qquad (3.1)$$

where

λ_j = random burst pedastal amplitude (3.2)

λ_b = background rate

$f(t)$ = low-pass waveform with peak equal unity

τ_j = occurrence time for j^{th} burst

ω_j = radian frequency proportional to one velocity component of the j^{th} particle.

We may write equation (3.1) as the sum of a constant, λ_b, a low-pass process, $\lambda_{\ell p}(t)$, (the pedastals), and a bandpass process $\lambda_{bp}(t)$. Then

$$\lambda(t) = \lambda_b + \lambda_{\ell p}(t) + \lambda_{bp}(t)$$

We assume that there are several fringes in the probe volume so that the spectra of $\lambda_{\ell p}(t)$ and $\lambda_{bp}(t)$ are non-overlapping. Now $\lambda_{bp}(t)$ is a zero-mean process, and $\lambda_{\ell p}(t)$ and $\lambda_{bp}(t)$ are uncorrelated. Thus we obtain

$$R_\lambda(\tau) = \langle\lambda(t)\rangle^2 + C_{\lambda \ell p}(\tau) + C_{\lambda bp}(\tau) \tag{3.3}$$

We now use the low turbulence assumption and further assume that the scatterers are uniformly dispersed in space so that, R(t), the rate of burst arrivals is a constant R. The results of Appendix A can be applied to derive expressions for the three terms in equation (3.3), the result

$$\langle\lambda(t)\rangle = \lambda_b + R\langle\lambda_j\rangle\int_{-\infty}^{\infty} f(t)dt \tag{3.4}$$

$$C_{\lambda \ell p}(\tau) = R\langle\lambda_j^2\rangle\int_{-\infty}^{\infty} f(t)\ f(t+\tau)dt \tag{3.5}$$

$$C_{\lambda bp}(\tau) = R\langle\lambda_j^2\rangle\frac{1}{2}\langle\cos\ \omega\tau\rangle\int_{-\infty}^{\infty} f(t)f(t+\tau)dt \tag{3.6}$$

where the expectation of the $\langle\cos\ \omega\tau\rangle$ term is with respect to the random variable ω_j. The derivation requires that we expand the product of cosines with the sum and difference formula and approximate the integral of the product of a low-pass term and a bandpass term as zero.

We now assume for this derivation that the turbulence is small and Gaussian with mean radian frequency ω_m and rms deviation σ_ω. Then by direct application of the definition of expectation we obtain*

*In general $\langle\cos\ \omega\tau\rangle$ is simply related to the statistical characteristic function for the random variable ω_j since this function is defined as a Fourier transform of the probability density function [7].

$$\langle \cos \omega\tau \rangle = \int_{-\infty}^{\infty} \frac{1}{\sqrt{2\pi}\,\sigma_\omega} e^{-(\omega-\omega_m)^2/2\sigma_\omega^2} \cos \omega\tau \, d\omega \qquad (3.7)$$

$$= e^{-\sigma_\omega^2 \tau^2/2} \cos \omega_m \tau$$

A simplified expression for the autocorrelation of the classical signal is thus

$$R_\lambda(\tau) = (\lambda_b + R\langle\lambda_j\rangle \int_{-\infty}^{\infty} f(t)dt)^2 \qquad (3.8)$$

$$+ R\langle\lambda_j^2\rangle(1 + \frac{1}{2} e^{-\sigma_\omega^2 \tau^2/2} \cos \omega_m \tau) \int_{-\infty}^{\infty} f(t) f(t+\tau) dt$$

This result shows that regardless of the shape of the envelope function f(t), the autocorrelation function has a cosinusoidal variation at the mean signal frequency providing all the previous assumptions are met.

The approach taken by Pike and others has been to further assume that the envelope function f(t) is also Gaussian to complete the derivation of the shape of the correlation function. In this case we assume

$$f(t) = e^{-t^2/\alpha^2} \qquad (3.9)$$

where α is the 1/e half width of the envelope and obtain

$$\int_{-\infty}^{\infty} f(t)dt = \sqrt{\pi}\,\alpha \qquad (3.10)$$

$$\int_{-\infty}^{\infty} f(t) f(t+\tau) dt = \sqrt{\frac{\pi}{2}}\,\alpha\, e^{-\tau^2/2\alpha^2}$$

The final simplified expressions for the first two moments of $\lambda(t)$ are

$$\langle\lambda\rangle = \langle\lambda(t)\rangle = \lambda_b + R\langle\lambda_j\rangle\sqrt{\pi}\,\alpha \tag{3.11}$$

$$R_\lambda(\tau) = \langle\lambda\rangle^2 + R\langle\lambda_j^2\rangle\left(1 + \frac{1}{2}\, e^{-\sigma_\omega^2\tau^2/2}\cos\,\omega_m\tau\right)\sqrt{\frac{\pi}{2}}\,\alpha\, e^{-\tau^2/2\alpha^2} \tag{3.12}$$

where

λ_b = background count rate
R = scatterer arrival rate
λ_j = random pedastal height from j^{th} scatterer
α = 1/e half burst duration
σ_ω = rms deviation of radian frequency due to turbulence
ω_m = mean radian frequency ($\sigma_\omega/\omega_m \ll 1$)
τ = delay variable of autocorrelation.

The shapes of typical correlation functions for zero turbulence and 10% turbulence are illustrated in Figure 3. We observe that functions of approximately this shape have been derived by others. We note that our derivation shows exactly where approximations and assumptions are used, and also reveals errors in the results by Pike et al. [15], who omitted the Gaussian term resulting from the pedastal.

3.2 IDEALIZED PHOTON CORRELATION OF LV SIGNALS

The number n_k is the number of photoelectron emission events in the interval which extends $\pm\Delta\tau/2$ from the instant $\Delta\tau$. An idealized photon correlator produces and sums delayed products from the uniformly spaced sequence $\{n_k\}$. We assume the total number of products accumulated is N. The accumulator produces a sum $\hat{M}_p$ at the delay value $p\Delta\tau$ given by

$$\hat{M}_p = \sum_{k=1}^{N} n_k n_{k+p} \tag{3.14}$$

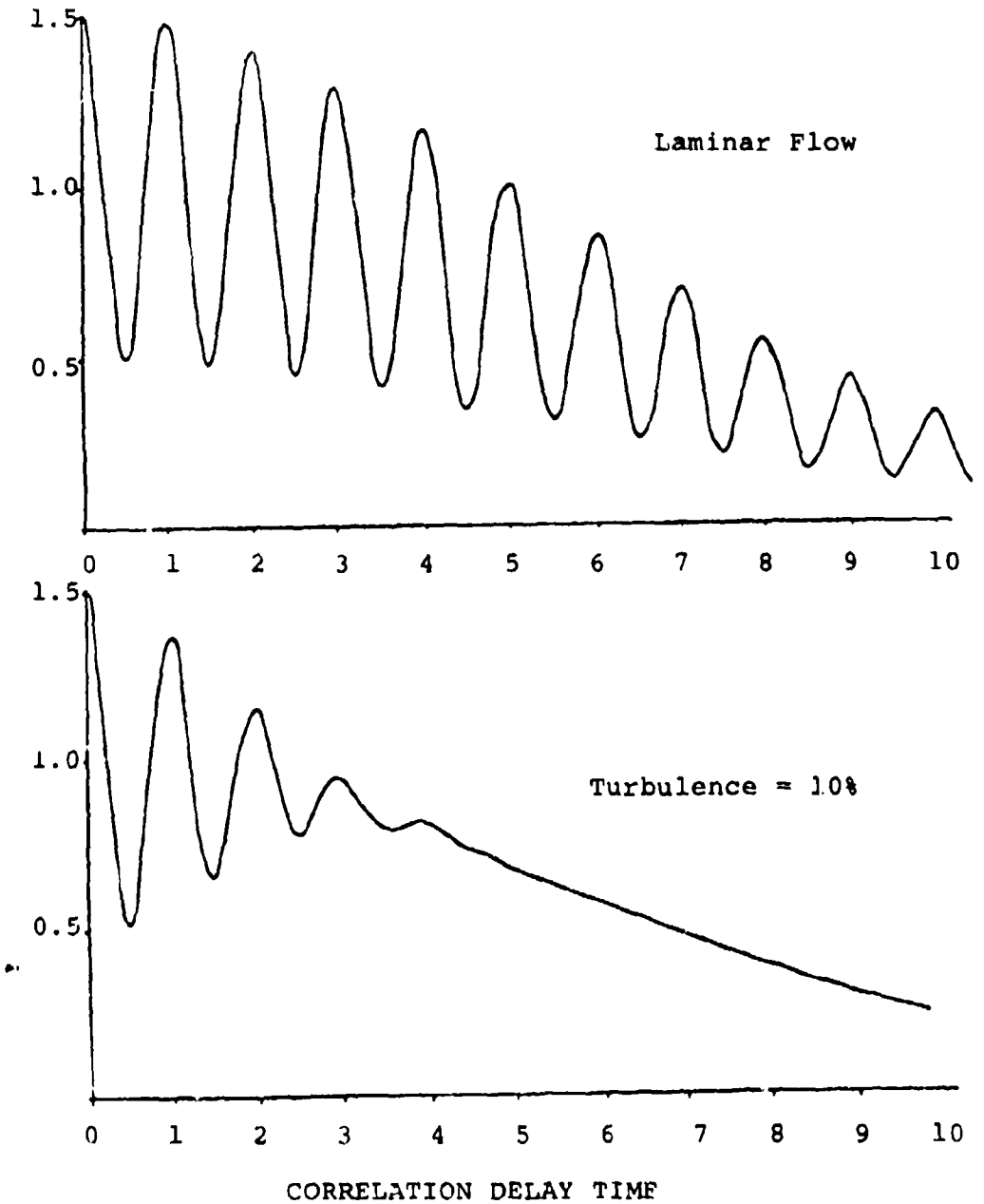

Figure 3. Autocorrelation Functions of Classical Burst Signals.

The unconditional expected value of this sum is obtained by interchanging expectation and summation as

$$\hat{M}_p = N\langle n_k n_{k+p}\rangle \tag{3.15}$$

$$= N\Delta\tau^2 R_\lambda(p\Delta\tau),\ p \neq 0$$

$$= N[\langle\lambda\rangle\Delta\tau + \Delta\tau^2 R_\lambda(0)],\ p = 0$$

where the last two lines of equation 3.15 are obtained from equation 2.27 under the assumption that $\Delta\tau$ is small compared with the details of $R_\lambda(\tau)$. We see that the zero delay term differs from the mean square value of λ by a predictable amount. The shape of the expected result is otherwise given by the function $R_\lambda(\tau)$ which may be interpreted via models such as that given in equation 3.12. When $\Delta\tau$ is not small compared with the details of $R_\lambda(\tau)$, then the result is smoothed according to equation 2.24. The difference between the $\Delta\tau^2$ multiplier in 2.27 and the $\Delta\tau$ multiplier in 2.24 occurs because the area under the triangular function $\Lambda(\tau/\Delta\tau)$ is just $\Delta\tau$.

3.3 A PHOTON COUNTING FREQUENCY DISCRIMINATOR

3.3.1 Basic Concepts

We will let the quantity $\hat{M}_{pq}$ be defined as follows

$$\hat{M}_{pq} = \sum_{k=1}^{N} m_k \tag{3.16}$$

$$= \left(\sum_{k=1}^{N} n_k n_{k-p}\right) - \left(\sum_{k=1}^{N} n_k n_{k-q}\right)$$

where

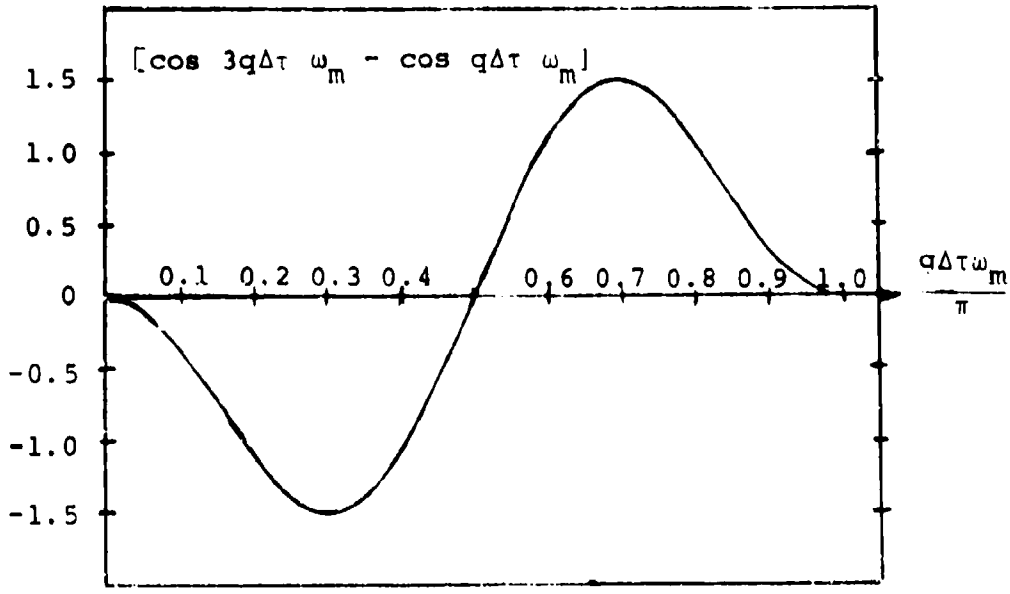

Figure 4. Discriminator Characteristic for Dual Correlate Approach.

$$m_k = n_k(n_{k-p} - n_{k-q}) \tag{3.17}$$

It is straight forward to show that, except for a few end terms which do not affect the result, M_{pq} is mathematically identical to the quantity $\hat{R}_p - \hat{R}_q$ where $\hat{R}_p$ and $\hat{R}_q$ are defined by equation 3.14. It is for this reason that we will lable the approach as the "Dual Correlate and Subtract" technique even though the delay values are negative instead of positive.* It is our purpose to now demonstrate that the expected value of $\hat{M}_{pq}$ behaves as a frequency discriminator as illustrated in Figure 4 under conditions which we will identify. The adjustment of the system clock period $\Delta\tau$ leads to a null in the expected accumulator value. Measurement of $\Delta\tau$ provides a direct measure of the mean signal frequency as we shall now show with our simplified signal models.

From equation 3.15 we obtain the expected value of the accumulator as

$$\langle\hat{M}_{pq}\rangle = N\Delta\tau^2[R_\lambda(p\Delta\tau) - R_\lambda(q\Delta\tau)] \tag{3.18}$$

The complete expression is obtained for our simplified signal model by using equation 3.12 in its entirety. Here we assume that $p\Delta\tau$ and $q\Delta\tau$ are both small compared with α so that the pedastal terms cancel as well as the steady term. This leaves

$$\langle\hat{M}_{pq}\rangle \approx N\Delta\tau^2 R\langle\lambda_j^2\rangle \frac{1}{2}\sqrt{\frac{\pi}{2}}\,\alpha \cdot \tag{3.19}$$

$$\cdot\left[e^{-\frac{1}{2}\left(\frac{1}{\alpha^2}+\sigma_\omega^2\right)(p\Delta\tau)^2}\cos\omega_m p\Delta\tau - e^{-\frac{1}{2}\left(\frac{1}{\alpha^2}+\sigma_\omega^2\right)(q\Delta\tau)^2}\cos\omega_m q\Delta\tau\right]$$

*$R_\lambda(\tau) = R_\lambda(-\tau)$

The negative delay implementation was more suitable for the hardware design.

Equation 3.19 appears to be complex. Now we choose to require that

$$p = 3q \tag{3.20}$$

and observe the behavior of equation 3.19 near the values of $\Delta\tau$ specified by letting $q\Delta\tau$ be one quarter of the signal period where both cosine terms will vanish.

$$q\Delta\tau = 2\pi/4\omega_m = T_m/4 \tag{3.21}$$

The shape of the term in braces is plotted in Figure 4 under the assumption of many fringes in the probe volume (α large) and low turbulence (σ_ω small). Thus the quantity plotted is simply

$$[\cos\ 3q\Delta\tau\ \omega_m - \cos\ q\Delta\tau\ \omega_m] \tag{3.22}$$

Figure 4 illustrates the expected behavior of the accumulator sum for changes in the mean signal frequency ω_m. If the system clock frequency is changed to change $\Delta\tau$, then the response is the product of $\Delta\tau^2$ and the curve shown in the figure. The shape of the curve is affected but the zero crossing locations are not.

3.3.2 Selection of Delay Constants

The theory of Section 3.3 does not uniquely specify the relationship of $\Delta\tau$ (the system clock period) to T_m the signal period. For a given value of signal period, T_m, the largest possible value of $\Delta\tau$ for an acceptable null is when $q = 1$ and $\Delta\tau = T_m/4$. This produces the least variability error (see section 6.0) and the most bias error due to time smear (the triangular weighting function in equation 2.24).

The value q = 1 also allows the highest signal frequencies to be measured for a given maximum system clock frequency.

The bias errors should be reduced at the expense of increased variability error and reduced maximum signal frequency by using q = 2, $\Delta\tau = T_m/8$. In order to facilitate experimental research, our design for a research instrument allows selection of p and q over a wide range.

4.0 HARDWARE PHOTON PROCESSOR

4.1 DESIGN RATIONALE

We have designed and constructed a feasibility prototype photon processor* to test the Dual Correlate and Subtract concept described theoretically in Section 3.0. Although this was a research system, it was designed so that it would outperform the existing Malvern photon correlator in several significant ways regardless of the feasibility of the Dual Correlate and Subtract concept. In this manner, we have assured that the AEDC would obtain an advanced photon processing system. In designing the system we have incorporated the following guidelines:

1. The design objective maximum clock speed was 100 MHz (10 nsec time resolution) with a guaranteed 40 MHz operation.
2. The system would utilize a four bit multiplier which operates at the clock frequency (down to 10 nsec per multiply) to avoid the ambiguities of interpretation of the single-clipping correlator.
3. The system was to be electronically switchable in configuration to provide a variety of different functions for different research and/or measurement purposes, including direct photon correlator.
4. The system would be designed to be computer compatible for extended dynamic modes.
5. The system and development costs would be minimized subject to the other goals.

In order to satisfy the cost and speed objectives the system was designed with MECL 10000 logic on special wire wrap panel. Significantly higher speed would have required

*Detailed design and construction provided by GW. Electronics, Atlanta, Ga.

the use of high-speed printed circuit board techniques and higher speed ECL logic. The use of printed circuit board techniques would have significantly increased the development time and hence costs. Although TTL circuits and techniques could have been used in a straight forward manner at lower speeds, the use of these circuits at 100 MHz would have been difficult or impossible and we chose the more expensive but faster MECL 10000 to avoid additional expense in design and debugging time.

A synchronous pipe line multiplier design was implemented which allows the 4 bit multiplication to be obtained via sequential shifts and additions. This multiplier technique requires the use of binary arithmetic. Simplicity and cost concerns then dictated that all high-speed switching and arithmetic be done in binary arithmetic. In order to minimize cost for the feasibility study while maximizing the system potential, the system was designed so that it could be operated by a person via toggle switches; and then, if feasibility were demonstrated, it could be conveniently interfaced to a minicomputer or special purpose dedicated microcomputer-controller for user oriented ease of control and data acquisition. The potential for microcomputer control will allow high-speed reconfiguration in the future for modes of operation not presently possible such as rapid sequential autocorrelation and multiple photon interval statistics.

4.2 SYSTEM DEFINITION

4.2.1 Overview

The delivered system, as illustrated in Figure 5, consists of an Ortec 9301 preamplifier, Ortec 9302 amplifier/discriminator, Ortec 401/402m minibin and power supply, a System Donner 6151 laboratory counter (SDC), a WAVETEK 1001A sweep generator (used as the variable local oscillator), and the SAI/GW Electronics Photon Processor.

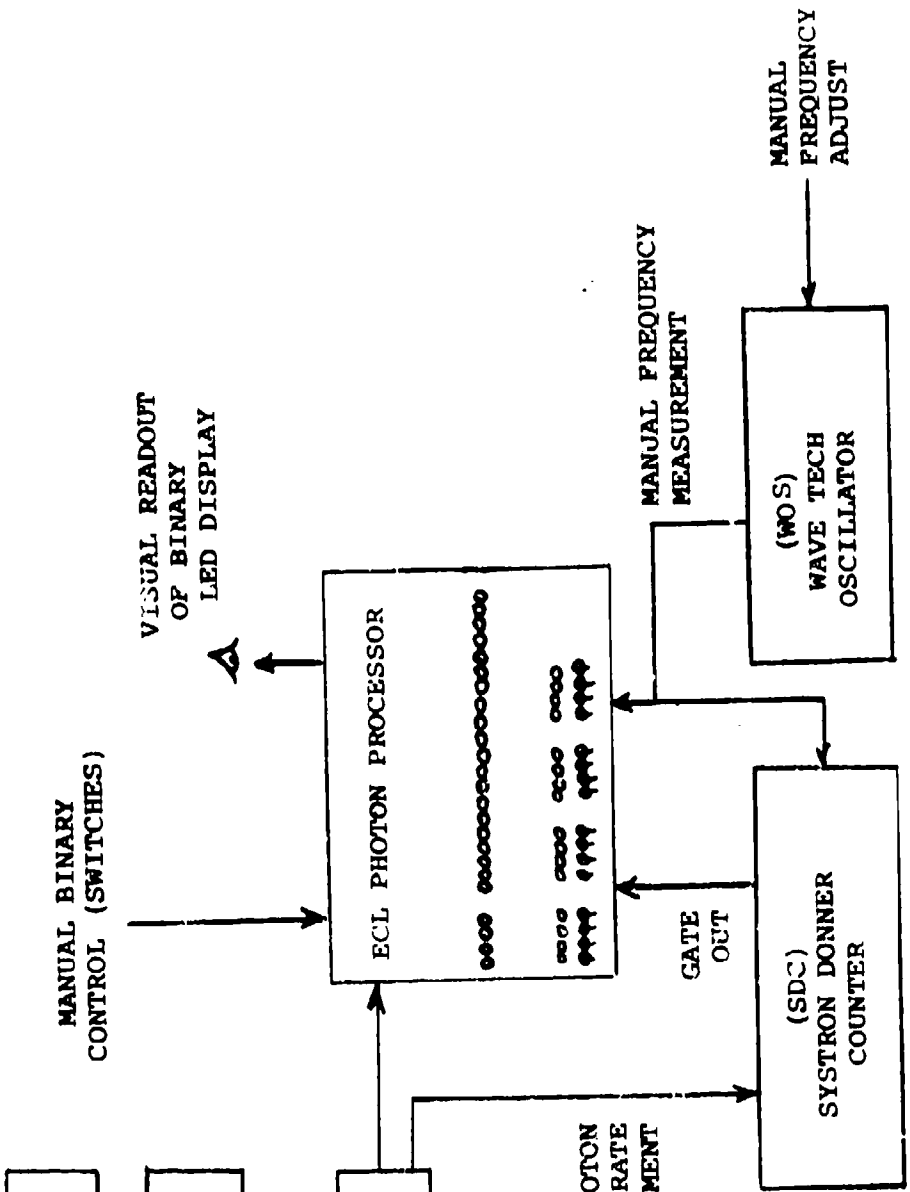

Figure 5. Feasibility Photon Processing System.

The SDC counts directly without prescaling to 200 MHz and has user installable options for computer interface cards for control and data acquisition. It is used both in diagnostics and system control and data acquisition. The WAVETEK oscillator is adjustable manually or by remote programming analog voltage over the range 500 KHz to 300 MHz. The Ortec preamplifier is required with a low-gain PMT such as an RCA 8644 and is helpful with a higher gain tube such as the RCA 931A. The preferred RCA tubes for photon counting are the RCA 8850 or C31024 tubes. The preamplifier is not required with these tubes (Tubes by other PMT Manufacturers have not been investigated. We do not claim any superiority for RCA. RCA tubes were available during the experimental work.) When used it is significantly important that the preamp be located physically directly at the PMT. The combination of any of the above mentioned photomultiplier tubes, and the Ortec preamp and amp/discriminator has a maximum speed of approximately 125 MHz with 112 MHz being a more reliable figure. (The dead time observed on an oscilloscope with PMT input to the 9302 unit was ≈ 9 nsec; output pulses were obtained to 125 MHz by driving the 9302 input with an oscillator and increasing the drive slightly at about 110 MHz.) The other major system component is, of course, the processor we designed and constructed. It is described in detail in the next section, and illustrated in Figure 7.

The coaxial cable used between the 9301 and 9302 units and its terminations are critical elements. We used precision 50 Ω cable and still found it desirable to use a 50Ω, 2x attenuator at the output of the preamp to reduce pulse reflections which can cause false discriminator correlations when a tube with large single photo-electron pulse variation is used.

By way of completeness we include a potential system diagram in Figure 6 which illustrates a proposed interface first with a microcomputer used in a minicomputer configuration and later with a micro processor controller and data acquisition system.

4.2.2 Input/Output

There are three BNC input jacks on the rear panel which are for the variable oscillator clock input, the output of the photon discriminator (ORTEC 9302) and the gate control pulse from the Systron Donner Counter. There are three output BNC's which provide decade scaled versions of the clock (÷ 10, ÷ 100, and ÷ 1000).

The front panel is illustrated by the photograph in figure 7. The top row of display lights consists of 5 LED's (left hand side) which continuously display the output of the 4 bit counter. The remainder of the top row of lights is the accumulator overflow, sign, and magnitude. The lower row of lights display the states of the control address (4 bits) the control data word (4 bits), the Read Address (4 bits) and the Read data (4 bits). The toggle switches under the lights correspond to the lights above. The separate toggle switch to the left provide an "enter" pulse to enter control data to a selected address or to change the read address. The two switches at the lower right are for addressing the control gate to either the system clock or the photon data stream.

4.2.3 Processor Circuit Description

Details of the circuits used in the photon processor have been provided to the Arnold Center in the form of schematic wiring diagrams which form a portion of a processor

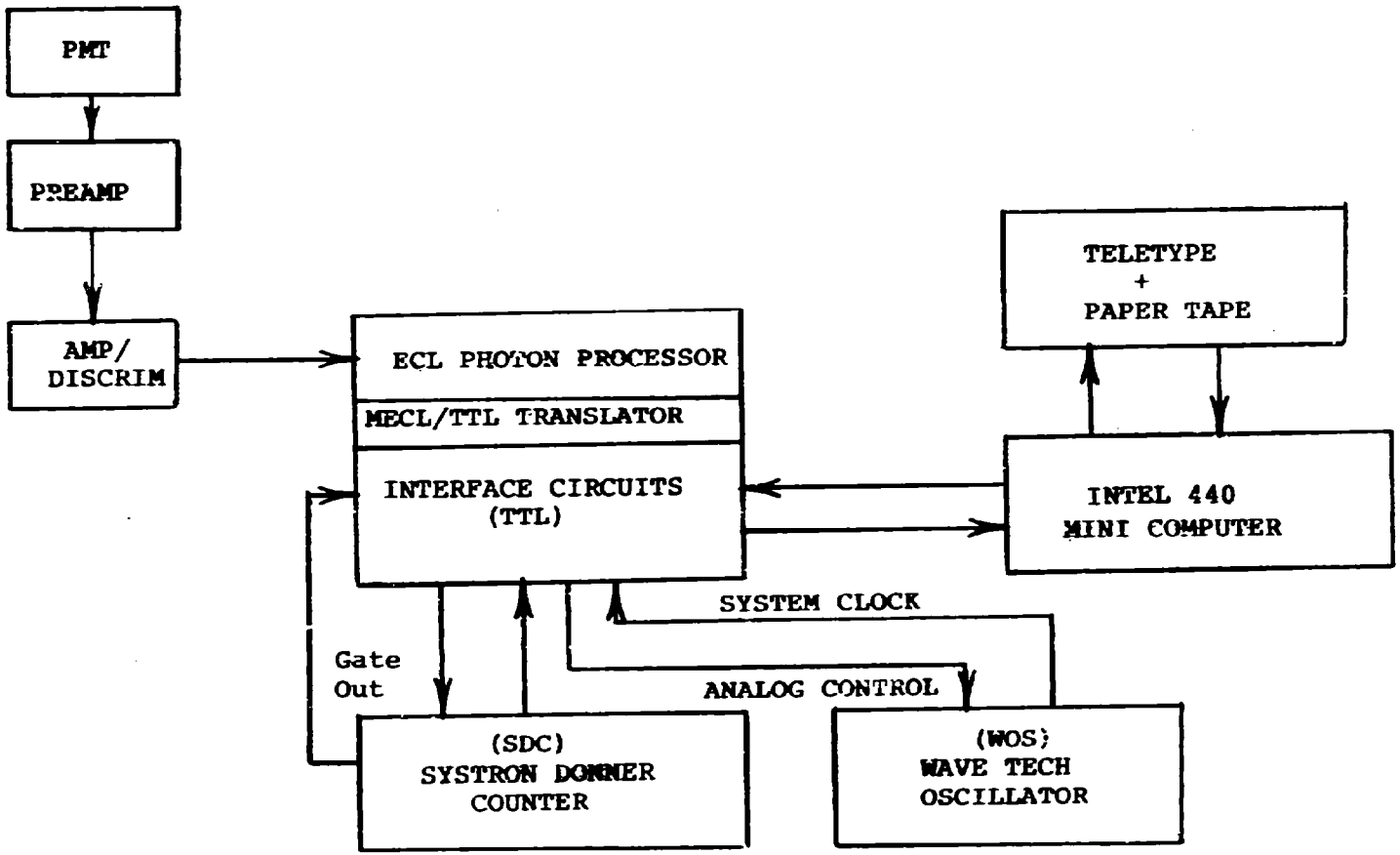

Figure 6. Proposed Extended System with Digital Counter.

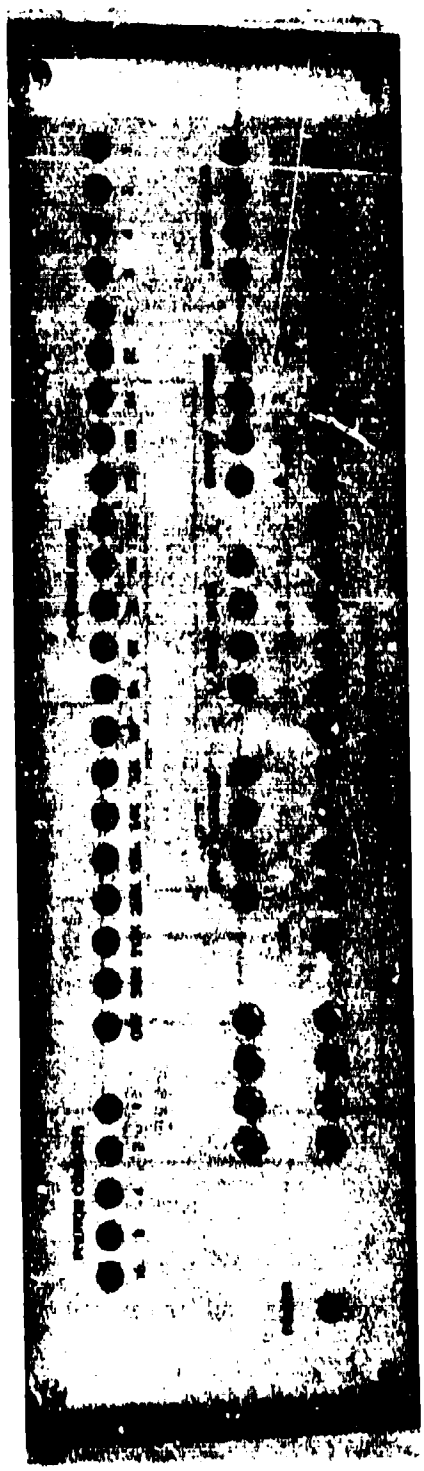

Figure 7. Photograph of Photon Processor.

manual deliveded with the feasibility processor. Figure 8 is a functional diagram which illustrates all internal subsystems. The following paragraphs describe the subsystem blocks illustrated in Figure 8. For Control and Read blocks not discussed below see the appropriate Control vocabulary definition in Section 4.2.4 or Read Vocabulary definition in 4.2.5.

Clock Shaping Circuit - The sinusoidal clock input is internally terminated with 50Ω. Shaping is accomplished by a flip-flop operated in a monostable mode. Timing is by propagation delay and a length of transmission line which is tuned for optimum clock pulse width.

3-Decade Scaler - has outputs at 1/10, 1/100, and 1/1000 of the system clock frequency. Outputs are in MECL logic levels and counting is synchronous.

SDC Control Circuit - provides resets and clears at the beginning of each measurement cycle to initialize the machine. The SDC Control Circuit also causes data to be held while the TTL input is low so that reading the front panel may be accomplished. Two switches on the front panel control options on the SDC control circuit. The switches are located at the lower right corner of the front panel and are labeled D and C. When placed in the up position they inhibit the Data and Clock respectively during the time the control input is low. In normal operation these switches are left in the down position.

Clock Tree - System clock distribution is by three packages of multiple output gates. This extensive clock buffering is necessary in spite of MECL's high low-frequency fanout capability due to the extreme speed of the clock pulse and the capacitive loading of the clock.

4-Bit Counter - This is a dual counter, that is one phase counts while the other is settled and connected to the comparator. There is a dead time of approximately 2 nsec

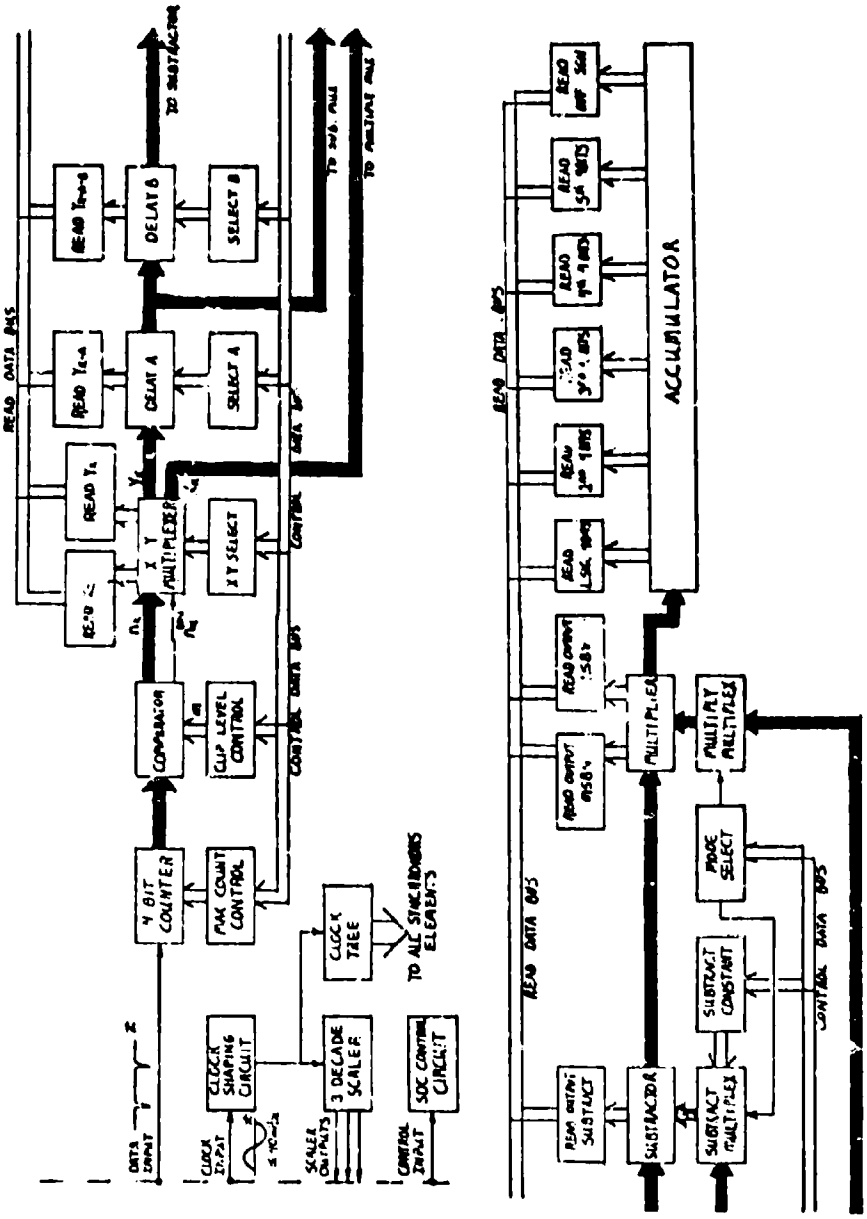

Figure 8. Subsystem Block Diagram of Photon Processor.

per clock period at the clock transition during which the counter switching occurs and any data will be ignored. The counter has a programmable stop at 1, 2, 4, 8, 15 and will never overflow into an erroneous state.

Max Count Control - Like all control words in the machine Max Count Control operates by entering a control word into the appropriate address.

Comparator - The Comparator or clipper compares the output of the 4-Bit Counter with a number from the Clip Level Control and assigns a binary value to $N_k^{(m)}$ based on the results of that comparison. If the photon count is greater than the programmed clip level then $N_k^{(m)}$ will be assigned a value of 1, otherwise $N_k^{(m)}$ will be assigned a value of 0.

Read X_k - causes X_k to be connected to the Read Data Bus as long as the correct address is held. For detailed information on read addressing and interpretation of output data see Section 4.2.5.

X Y Multiplexer - selects either clipped or unclipped data and transmits this to Y_k lines and X_k lines in any combination.

Delay A - This is a digital delay line with a length chosen by a decoder. All data passes through all twelve delays and is lost when clocked out of the twelfth position.

Delay B - Similar to Delay A, this delay element has taps at 0, 2, 4, and 8.

Subtractor - Subtracts the output of the Subtract Multiplex from the output of the Delay B. Subtractor is on two's complement arithmetic but both inputs are positive so no input conversion is required. Output is five bits (4 bits plus sign) and is converted to sign and magnitude representation for the multiplier.

Subtract Multiplex - causes either Y_{k-A} or the Subtract Constant to be subtracted from Y_{k-A-B} based on the state of the Mode Select.

Subtract Constant - is a register storing a constant entered as a control word. See Section 4.2.4.

Mode Select - is two bits of information stored in order to define the state of the Subtract Multiplex and the Multiply Multiplex. It is entered as a control word. See Section 4.2.4.

Multiplier - multiplies the outputs of the Subtractor and the multiply Multiplex. Arithmetic is in signed magnitude. The Multiplier is a fully pipelined shift and add design.

Multiply Multiplex - selects either X_K or 1, as one input to the Multiplier based on the state of the Mode Select.

Read Accumulator - accomplished sequentially by 5 separate Read control addresses (or visually directly from LED display). See Section 4.2.5.

Accumulator - This is a pipelined synchronous accumulator in two's complement arithmetic. Conversion of the input to two's complement is by exclusive or gates and a carry into the first stage. The overflow signal is generated by OR-ing together three bits more significant than the most significant bit displayed or available through reads. This means that it is possible for instance to overflow positive and add on enough negative to come out of overflow. Output conversion to signed magnitude representation is by exclusive or gates and therefore all negative numbers are in error by a one. This error is small compared to the width of the accumulator and its correction does not justify the amount of circuit complexity which would be required.

4.2.4 Control Vocabulary

Control is provided by programming control words into various addresses. The addresses and definition of the

meaning of the various control words are given in Table 1.

4.2.5 Read Vocabulary

When a Read address is entered, four bits of data are continuously displayed by the LED data lights. For computer controlled operation, the clock would be stopped, and then the various addresses would be read. The addresses and data definitions are given in Table 2.

4.3 MODES OF OPERATION

The SAI processor may be operated in static modes at present. It has the potential for operating in dynamic modes. A static mode is one in which the machine configuration is selected by hand or by computer control and then data is taken for some length of time. A dynamic mode is one in which the SAI processor is rapidly re-configured during the data collection process by computer control. Some of the static modes are: 1. Mean; 2. Mean Square; 3. Single Point Correlation; 4. Single-Point Cross-Correlation; 5. Dual Correlate and Subtract. There are other static configurations and many possible dynamic modes. Some of interest are: sequential autocorrelation, counting probability histogram, diagnostic sequences, and others. We are establishing here the procedures and machine codes and sequences which produce the static modes of operation just listed.

Our basic approach for static modes is as follows:

1. Establish the Dual Correlate Mode with a basic set of the optional choices..take data or reconfigure as follows.
2. Select other static modes
3. Select other optional choices.

CONTROL ADDRESS	ELEMENT NAME	DATA WORD	SELECTION
0000	RESERVED FOR FUTURE OPTIONS		
0001	RESERVED FOR FUTURE OPTIONS		
0010	4-bit counter	0000	Stop at 1
		0001	Stop at 2
		0011	Stop at 4
		0111	Stop at 8
		1111	Stop at 15
0011	Comparator	abcd	(abcd) = m = clip level (0-15) n(m) = 1, n>m; = 0, n≤m
0100	XY Multiplex	00xx	X = Full, Y = Full
		01xx	X = Full, Y = Clipped
		10xx	X = Clipped, Y = Full
		11xx	X = Clipped, Y = Clipped
0101	Delay A	0000	Delay = 0 clock periods
		0001	Delay = 1 clock periods
		0010	Delay = 2 clock periods
		0011	Delay = 3 clock periods
		0100	Delay = 4 clock periods
		0101	Delay = 5 clock periods
		0110	Delay = 6 clock periods
		1000	Delay = 8 clock periods
		1001	Delay = 9 clock periods
		1010	Delay = 10 clock periods
		1100	Delay = 12 clock periods
0110	Delay B	xx00	Delay B = 0
		xx01	Delay = 2
		xx10	Delay = 4
		xx11	Delay = 8
0111	Mode Select	xx00	subtract constant, multiply by 1
		xx01	subtract constant, multiply by x_k
		xx10	subtract Y_k-A, multiply by 1
		xx11	subtract Y_k-A, multiply by X_k
1000	Subtraction Constant	(abcd)	Positive binary word (0-15) equal to subtraction constant
1001 to 1111	RESERVED FOR FUTURE OPTIONS		

Table 1 Control Vocabulary.

ADDRESS	READS LOCATION	MEANING OF BITS			
		8	4	2	1
0011	X_k	8	4	2	1
0100	Y_k	8	4	2	1
0101	Y_{k-A}	8	4	2	1
0110	Y_{k-A-B}	8	4	2	1
0111	SUBTRACT OUTPUT	SIGN	8	4	2
1000	MULTIPLIER MSB's	128	64	32	16
1001	MULTIPLIER LSB's	8	4	2	1
1010	ACCUMULATOR LSB's	8	4	2	1
1011	ACCUMULATOR 2nd 4 Bits	128	64	32	16
1100	ACCUMULATOR 3rd 4 Bits	2K	1K	512	256
1101	ACCUMULATOR 4th 4 Bits	32K	16K	8K	4K
1110	ACCUMULATOR 5th 4 Bits	512K	256K	128K	64K
1111	ACCUMULATOR OVERFLOW AND SIGN	X	X	SGN	OVF

Table 2. Read Vocabulary

4.3.1 Establish Dual Correlate Mode

The following basic sequence removes the max count limits, the single clipper, and sets the delays for eighth period increments. (Quarter period increments would be A = 1, B = 2, instead of A = 2, B = 4). The machine computes

$$m_k = n_k \ (n_{k-A-B} - n_{k-A})$$

The code is entered as shown in Table 3.

ADDRESS	DATA	OPERATION
0010	1111	max count = 15
0011	0000	clip level at zero
0100	00xx	full multiply
0101	0010	delay A = 2
0110	xx10	delay B = 4
0111	xx11	subtract Y_{k-A} and multiply by X_k
1000	0000	subtract 0

Table 3. Dual Correlate Mode.

4.3.2 Select Other Static Modes

From the basic static mode, single codes are used to change modes to the ones indicated in Table 4.

MODE	FUNCTION m_k	CONT. ADDRESS	DATA
mean	n_{k-A-B}	0111	xx00
mean square	n_k^2	0111	xx01
		0101	0000
		0110	xx00
autocorrelate	$n_k\ n_{k-A-B}$	0111	xx01
	set delay	0101	abcd
		0110	abcd

Table 4.0 Other Static Modes

4.3.3 Clipping and Other Options

A variety of optional choices are allowed by the processor logic. The following listing gives several of the most likely to be used options.

4.3.3.1 Cross Correlate with Clipped Sequence. In any mode the clipped version of n_k (which is $n_k'^{(m)}$) may be applied to either the Y_k or X_k branches. A clip level should also be selected. These choices are made with control addresses 3 and 4 (0011 and 0100). See machine language Table 1.

4.3.3.2 Max Count. The maximum value of n_k may be restricted to 1, 2, 4, or 8 instead of 15 by using the desired max count number as the data word to address 2 (0010).

4.3.3.3 Set Delay. For the autocorrelate mode the delay is the sum of delay A and delay B. The data word for the A delay is equal numerically to the delay excluding 7, 11, 13, 14, 15). The data word for the B delay is the log base 2 of the delay.

4.3.3.4 Subtraction Constant. If a constant other than zero is to be subtracted it should be loaded into control register 8 (0100). This feature is provided to reduce the mean-square level stored in the accumulator when the autocorrelate mode is used and the steady optical power component is large compared with the time fluctuating component.)

4.4 OPERATING PROCEDURES

A manual measurement with the photon system requires several operations with the Wavetek oscillator, the laboratory counter, and the 9302 discriminator. These are described briefly here.

4.4.1 Discriminator Threshold

The combined gain of the PMT, the preamp, the attenuation (if any), the amplifier portion of the 9302, and the discriminator threshold must be chosen to satisfy the following requirements: a) maintain speed b) avoid saturation of amplifiers by large photoelectron pulses c) avoid missing small photoelectron pulses d) avoid setting threshold down into the amplified Gaussian electronic noise from the preamp or the ringing tails of the larger single photoelectron pulses. In practice, these constraints could not all be met simultaneously with either the RCA 8644 or the RCA 931A tube due to the large range of amplitudes of the single photoelectron pulses. In the future better photon counting tubes should be used.

4.4.2 Adjustment of Clock Frequency and Use of Counter

For an autocorrelate mode the Wavetek oscillator frequency is adjusted by using the laboratory counter to

accurately determine a convenient delay resolution increment. The oscillator is then left at that frequency while the measurement is made at different delays. For the Dual Correlate Mode, the clock frequency is adjusted by an operator receiving feedback from the accumulator display lights until a null is reached, then the oscillator frequency is read with the laboratory counter to determine the clock frequency accurately. This feedback can either be with the processor running continuously (best for very low photoelectron rates) or repetitively for fixed duration gate intervals provided by the lab counter output gate. In either case, the "B" counter of the lab counter is counting its internal crystal oscillator so that the "A" counter may be used to count the total number of discriminator output pulses during the gated interval. (There are two isolated but equal outputs of the ORTEC 9302 Amp/Disc.). This simultaneous count may be used for normalization purposes.

5.0 EXPERIMENTAL MEASUREMENTS

Four different sets of measurements were made during the contract period. The details of all of these measurements have been documented in informal monthly progress reports. Only the general nature of the experiments and significant data are summarized briefly here.

5.1 PRELIMINARY MEASUREMENTS

This set of experiments were conducted in October 1974 prior to the construction of the photon processor.

5.1.1 Photomultiplier Tubes

Several different types of observations were made with RCA 8644, 931A, and 8850 photomultiplier tubes. First, observation of single photoelectron pulses on a fast oscilloscope demonstrated the advantage of the 8850 tube over the other two. When observing the brightness of the oscilloscope display versus amplitude of the pulses there is clearly a preferred amplitude with a ±15-25% standard deviation (qualitative judgement) for the 8850 tube. The other two tubes produce the brightest display at zero amplitude, actually at the trigger level, with gradually decreasing brightness with increasing amplitude. With the 8850 tube it was easy to set a threshold trigger level above the electronic noise and below the minimum pulse amplitude of most of the pulses. This was not possible with the other two tubes. The pulse amplitudes from the 8850 was approximately 100 times that of the 8644 with the voltages used.

No preamp was needed with the 8850 tube.*

Two RCA 8644 photomultiplier tubes assemblies were tested for absolute anode sensitivity, quantum/collecting efficiency product, and qualitative waveform features. The first unit was an unlabled, flat black assembly which we designate Model 0. The second unit was PMR-20, serial 1. Both units were tested at a supply voltage of 1800 v at the green argon laser wavelength (514.5 nm). The pulse waveform of the Model 0 unit exhibited considerably more ringing and therefore less threshold triggering stability than did the PMR-20 unit. The measurement results are provided below in Table 5. We note that while the anode sensitivity results are needed for calibration purposes in the burst height distribution studies, it is the η quantity which limits both photon-counting and burst counter processors since variations in DC dynode gain are easily compensated by preamplifier gain and do not affect the signal-to-noise ratio.

	Anode Sens Amps/watt	η method 1	ηF method 2
RCA typical (spec)	16,600	(0.125)(0.8)=	0.10
Model zero	18,600	0.10	0.07
PMR-20	10,600	0.035	0.04

Table 5. Measurement Results

*Despite the clear advantages for photon-counting, the 8850 tube was not suitable for use with signals large enough for burst-counter operation due to saturation of the dynode divider current. This could be remedied by changing the dynode divider to provide more current, but this was not done during the contract period. Hence the poorer tubes were used in later photon counting experiments where comparison with a burst counter processor was desired.

5.1.2 False Triggering of Burst Counter

An experiment was performed in which an ARO Model 8 Burst Counter processor was used with a laboratory LDV experiment. At low signal levels with low trigger threshold settings on the oscilloscope used for triggering the processor, a significant fraction of the trigger events were from anomalously large single photo-electron pulses (RCA 8644 tube again). Significant improvement in trigger reliability was obtained by using a low pass filter in the trigger circuit with bandwidth from 2 to 4 times the pedastal bandwidth. This is much less bandwidth than is needed for the AC signals. The technique is only effective when the mean signal visibility is high since the pedastal is used for triggering. Such techniques would not be necessary with larger PMT stage gain and smaller pulse height variation.

5.1.3 Photon Correlation Demonstration

Mr. Bob Koelzer and Mr. Charles Sheckells of Honeywell Saicor provided a demonstration of the model SAI 43A digital correlator with photon correlation option. A laboratory LV system was set up with an ARO model 8 burst counter processor for comparison. An RCA 8644 PMT was used in the experiment. The experimental arrangement consisted of a forward scatter, fringe type LDV system with the probe volume located respectively three inches and one inch in front of the intake of a small laboratory wind tunnel. In the first test the optical system consisted of a small 1.6 mw He Ne laser, 50-50 self aligning splitter blocks, a 12.1 cm fl transmit lens, a pair of 19.2 cm lens in a one-to-one imaging arrangement, a folding mirror, and an RCA 8644 PMT with a pinhole and laser line filter.

A second test was conducted with the optical system changed in the following manner:

Transmit focal length = 62 cm
Pinhole diameter = 400μm
Half-angle between beams = 1.17°
Fringe Spacing = 15.4μm
Probe Volume Diameter = 400μm

Other system parameters were unchanged except as noted below.

In the conduct of the second test, burst counter data was first taken with the system as described; then a 10 x area ratio restricting aperature was placed over the collecting optics to reduce the collecting aperture to f/11.7. Under these conditions both burst counter and photon correlator data were taken (12 minutes of burst counter data followed by 15 minutes of correlator data (real time equivalent 0.375 sec). Data sets were obtained with a short (12.1 cm) and a long (62 cm) transmitter configuration, both forward scatter, using a 1.6 mw He Ne laser, unseeded natural air, at velocities of 0.91 m/sec and 5.8 m/sec respectively. Burst counter measurements with printer output were also made for each optical geometry and flow velocity. The mean period and rms deviation have been computed from 60 values of the burst counter data (before 10x attenuation) for comparison with photographic records of the photon correlator display; these are shown in the following table. The data collection time for the correlator is unknown for the 12.1 cm transmit lens case, but was approximately 30 minutes. The time for the 62 cm results was 900 seconds (0.375 seconds, real time equivalent), with the good data rate from the burst counter being 0.2/sec in this latter case (with 10x attenuation).

Transmit Lens Focal Length	Velocity	Fringe Period	Mean Period Photon	Mean Period Counter	Standard Deviation Counter
12.1 cm	0.91m/sec	3.0 μm	3.2±0.1 μsec	3.29μsec	0.22
62 cm	5.8m/sec	15.4 μm	2.6±0.1 μsec	2.66μsec	0.05

Table 6. Photon Correlation Demonstration Results.

The experiment indicated that the photon correlator provided a more sensitive detection technique than the ARO processor. The time required would have been less if tne correlator multiplier could have been fast enough for real time data processing.

5.1.4 Distributions of Burst Rate Vs. Amplitude

Low speed measurements were made to determine the distribution of LV signal burst amplitudes for a 147 mw backscatter Argon LV system as illustrated in Figure 9. The parameters of the system were chosen similar to those expected in future Arnold transonic windtunnel tests. Absolute quantities were measured so that the data could be scaled* to typical transonic velocities and so that the magnitudes could be related to particle size through Mie theory predictions. In order to relate the detected signal amplitudes to absolute scattered power, it was necessary to calibrate the photomultiplier tube assembly with regard to absolute anode sensitivity. In order to relate the electrical levels to photoelectron rate, it was necessary to measure the product of quantum efficiency and collection efficiency of the PMT. These measurements have already been discussed. Extreme care was used in eliminating low-level ground loops, room light effects and DC signal drifts. The measurement was made with very low velocity (1.8 m/sec) and filter bandwidth chosen to pass only the pedastal. This was done after observation of the signals at wider bandwidth showed that they had good fringe visibility. The extreme low-pass filtering was accomplished using the filter in a TEKTRONIX 1A7A plug-in unit as illustrated in Figure 10. The sweep speed was made just fast enough to nearly fill the display with a single burst so that few were missed. (The bursts remained non-overlapping, except in rare events, down to the lowest levels measurable (5 μ volts).

*See "Scaling" in Appendix B.

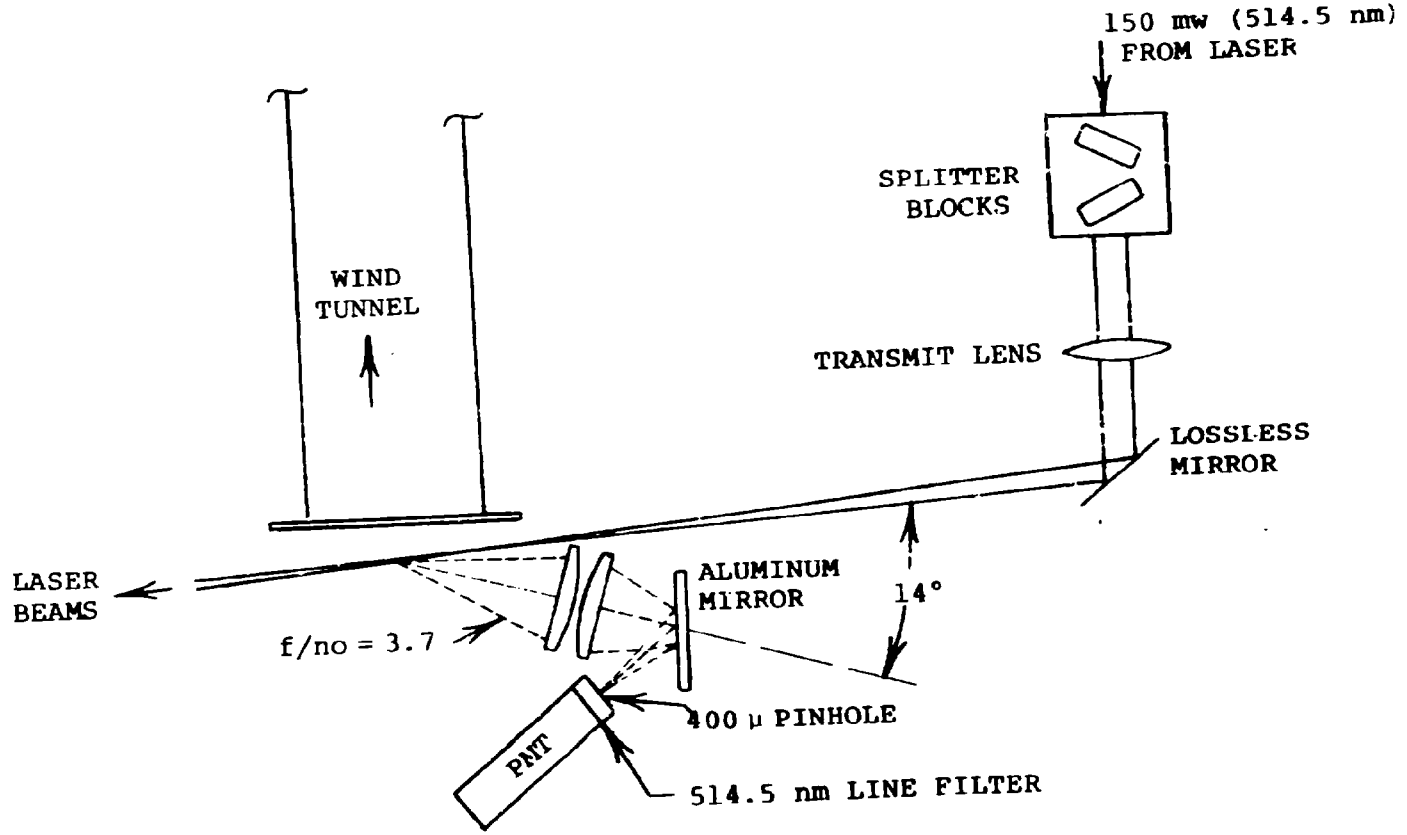

Figure 9. Optical Setup for Burst Height Distribution (Top View).

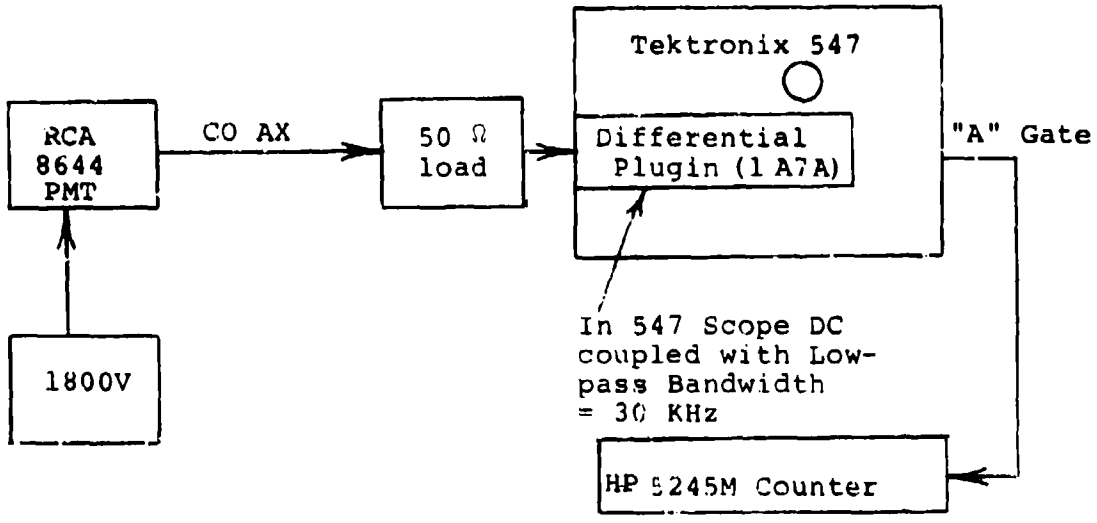

Scope Sweep = 10 μsec/div
total sweep time = 100 μsec

Note: RMS "Grass" noise ≈ 1 μv rms

Figure 10. Electronic Arrangement for LV Burst Height Measurement.

Figure 11 summarizes the results of cumulative rate/amplitude measurements obtained using the argon back-scatter system just described. The procedure included using low velocity and low filter bandwidth to obtain amplitude measurements from particles which would only scatter a few photons during the short transit time at typical transonic velocities. Ten-second counts were made at each trigger threshold settings. Three consecutive runs made over a period of 1½ hours showed excellent agreement and repeatability.

Particle size computations were made based on the n = 1.55 Van DeHulst curves. The parallel polarization values at 166° scattering angle were used to be consistent with the experiment. Also, calibrated PMT and optical system parameters were used. The right hand bars in Figure 11 are the calculated values for a particle through the center of the probe volume. The left hand bars are $1/e^2$ values of amplitude that show the minimum peak amplitude that the same particle size could produce. (The collecting optics pinhole was matched to the $1/e^2$ pulse diameter.)

5.1.5 Scaling of Burst Amplitude Data

The optical parameters of the laboratory burst amplitude (a_j) distribution measurement were chosen as closely as possible to coincide with future 4T transonic wind tunnel optics after discussion and with the help of Mr. Don Brayton. The wavelength, beam intersection angle, and focal beam diameters were nominal. Velocity, laser power, and collecting f/no must be scaled. The two largest unpredictables are the difference between the natural aerosol in the lab test and the transonic test and the differences in on-axis backscatter and small-angle off-axis backscatter with regard to probe volume size and definition. Neglecting the last two factors (although they are significant) we can scale velocity, laser power, and collecting f/no to obtain a typical data set.

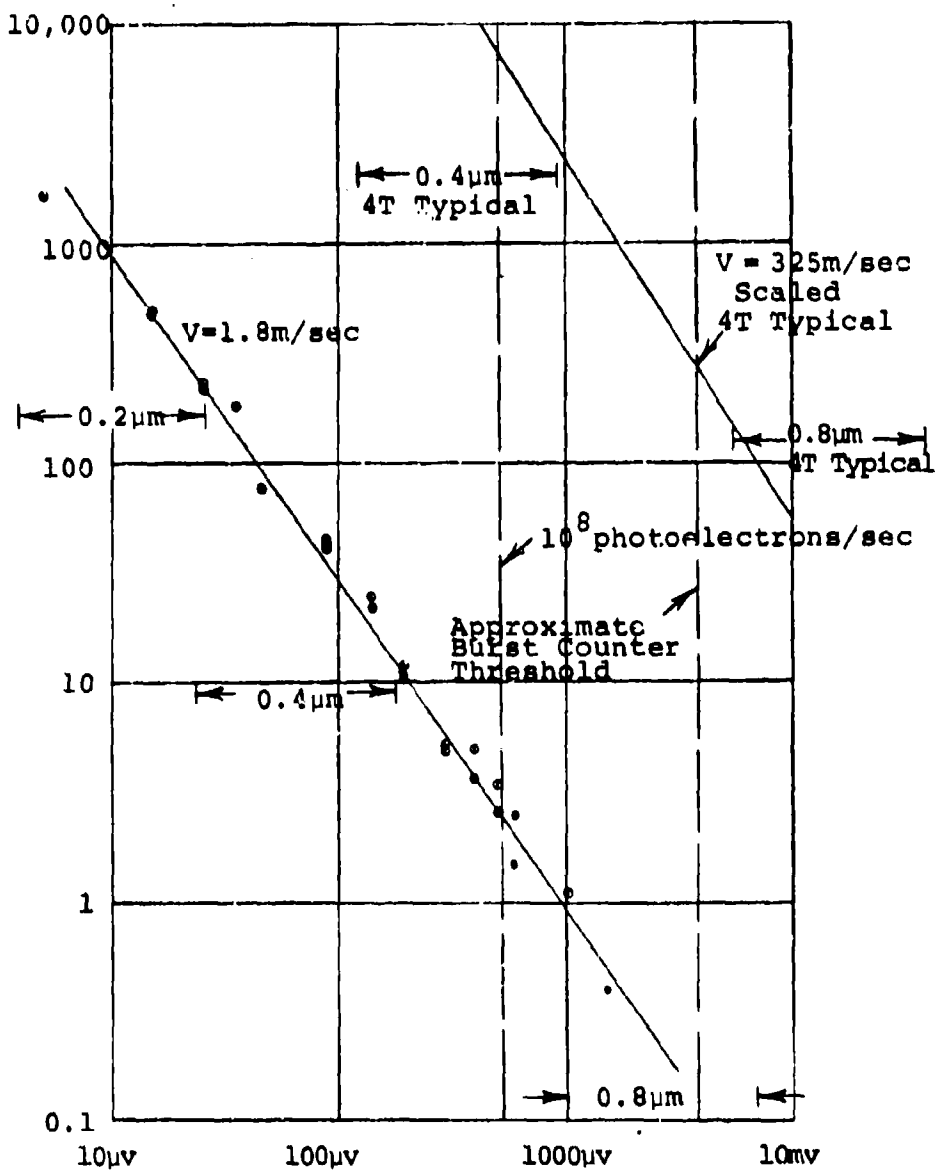

Figure 11. Burst Amplitude Data for Low-Speed Natural Air (1.8m/sec) and Data Scaled to 325 m/sec.

The assumed scaling parameters are given in Table 7.

	Lab	4T	Ratio
Velocity	1.8m/sec	325m/sec	180.6
Signal Frequency	143 KHz	25.8 MHz	180.6
Signal Period	7 sec	39nsec	5.54×10^{-3}
Burst Duration	175 sec	0.969 sec	5.54×10^{-3}
Collecting f/no	3.7	6	0.62
Laser Power	150mw	2w	13.3
Quantum Efficiency*	0.04	0.12	3

Table 7. Scaling Burst Amplitude Data.

The procedure is as follows: The data rate at a given value of a_j is scaled by the velocity (180). The value of a_j at a given rate is scaled by the laser power and the square of the f/no ratio (5.1). Thus the log-log plot is the same but translated up by the velocity and translated to the right by the power ratio. The particle size bars are translated in the same manner. The result of these operations is illustrated by an additional line in Figure 11.

The data given in Figure 11 in load voltage may be converted to the more significant quantity λ_j the peak pedastal photoelectron rate in photoelectrons/sec by the formula

$$\lambda_j = \frac{a_j \eta}{h\nu(50\Omega)S_a} \tag{5.1}$$

where for the tube used (see PMR-20, Table 5) we obtain $\lambda_j = 2.0 \times 10^{11} a_j$. Figure 11 indicates the locations of the $\lambda = 10^8$/sec rate (maximum for state-of-the-art photon-counting) and also a line corresponding to the lower limits of burst counters with a 25 MHz signal frequency.

---

*including collecting efficiency. This assumes use of RCA 8850 in 4T.

5.2 BACKGROUND AND SIGNAL LEVEL EXPERIMENTS

In April of 1975 a trip was made to the Arnold Center to check out the Ortec and Systron Donner equipment and the photon counter portion of the experimental processor. In addition we wished to observe photon signals from a back-scatter LV system which Virgil Cline and others at the Arnold Center had constructed for use in the 1T transonic wind tunnel. The maximum photon discriminator pulse rate is just over 100 MHz so it was important to see what the rates were from a typical real LV system.

5.2.1 Equipment Checkout

The Wavetek oscillator (WOS) was used to drive the Systron Donner Counter (SDC). The SDC operated in linear agreement with the dial reading of the WOS to 230 MHz. The WOS was applied to the amplifier discriminator with the SDC counting the discriminator output pulses. This produced reliable behavior to 100 MHz with low level input (unrecorded); with increased amplitude, the range was extended to 125 MHz.

The RCA 8644 and 8850 tubes were not used during this trip. Virgil Cline's set-up included an RCA 931A so this tube was used exclusively. A variety of arrangements of 50 Ω cables, attenuators, terminators, cable lengths, and amplifier combinations were tried out to minimize after-pulse ringing which was at first a serious problem. The bandwidth restriction and pulse shaping effects of the 9302 amplifier increase the pulse width slightly from that amplified and delivered by the 9301 preamp, but also reduces the high-frequency ringing.

The effect of varying the discriminator threshold was observed. This experiment dramatically demonstrated the significance of the pulse height variation. When the threshold was set low (50-100 mv after 10x preamp and 20x amp), the oscilloscope revealed secondary firings of the

discriminator at the spacing of the first round-trip pulse reflection ≈ 20 nsec (even with all the precautions of precision cable and terminations). The secondary pulses were caused by the large single-photo-electron pulses whose reflections were also above the threshold. These were removed successfully by setting the threshold up to 400 mv. The counted photon rate (disc out to SDC) decreased by a factor of 20.

The result of the threshold experiment shows that

(a) The 931A cannot be efficiencly used for fast photon-counting work because pulse-height variation forces one to set the threshold so high that most of the signal pulses are missed.

(b) The experiment of comparing the 8850 with other tubes for count rate cannot be performed with any meaning until criteria for secondary threshold crossings are defined. In photon correlation work this criteria is expected to be so stringent that the effective useable quantum efficiency of the 8850 will be many times greater than the 931A.

ORTEC 9 specifies nsec as the typical dead-time for the 9302 amp/discriminator and guarantees 10 nsec maximum. Driving the input with an oscillator and getting output pulses at 125 MHz would seem to indicate an 8 nsec dead time for the unit we obtained. However, when the discriminator output was observed on the oscilloscope at high light levels ($\lambda = 50 \times 10^6$) the minimum separation observed between the triggering pulse and the next one was 9 to 10 nsec. We consider the combined experiments to verify the "typical" number of 9 nsec.

Check out of the photon counter indicated that it was only performing satisfactorily to count rates of about 60 MHz. The circuitry was later redesigned and reconstructed to operate to over 100 MHz count rates.

5.2.2 Background Rates

This was a significant experiment. We wished to determine background rates that could be expected with a practical LV optical set-up in use at the AEDC. With 50 mv discriminator threshold (RCA 931A with 200x amplification before the threshold) we obtained the following results by counting the discriminator pulses with the Systron Donner counter.

	Condition	Rate
1.	PMT covered (Dark)	0.10 MHz
2.	Room lights out and black curtain in front of window	0.15 MHz
3.	Room lights off, window light on wall in field of view	1.0 to 2.5 MHz
4.	Same as (3) but with laser on (signal from natural air)	≈ 25 MHz
5.	Same as (3) but with over-head room lights on	≈ 50 MHz
6.	Same as (4) but with typical plexiglass window inserted in beams. (No noticeable change.)	≈ 25 MHz

The signals obtained are in an acceptable range of rates for photon counting. The exception was the background count with the room lights on. This experiment shows the need for careful shielding of the PMT optics.

5.3 FEASIBILITY DEMONSTRATION OF THE DUAL CORRELATE AND SUBTRACT MODE

On September 2, 1975 a trip was made to the Arnold Center with the experimental photon processing system. Although deterministic laboratory checkout had indicated that all the developmental bugs had been eliminated from the circuitry, this was not the case. Additional debugging of the circuits was required. No measurements were obtained until the last half of the day September 5, 1975. The system

was used that day to make mean flow measurements in a small laboratory jet under weak signal conditions where the ARO Model 8 burst counter processor would not make any measurements. A small amount of data was obtained for bias error and variability error evaluation. The mean velocity estimate differed in one instance by 4% from the velocity measured by the ARO counter at 3 times greater laser power. This is good agreement since the ARO processor was barely producing data (1 data point validated per 3 seconds at the higher power).

The variability error agreed very well with the variability theory which is discussed in section 6.0. The experiment is described in more detail below.

5.3.1 The Experiment

An off-axis backscatter (fringe-type) LV system operating with a wavelength of 514.5 nm and fringe spacing of 6.9 micrometers was assembled for a laboratory test with a pipe jet air flow (20 ft/sec, mean velocity). The shop air jet appeared visually to scatter less light than the room air so that the beam crossing location was nearly invisible in comparison with the other beam locations. After alignment, unusually weak signals were obtained from an RCA 931A PMT even with 1.7 watts of laser power. When a low-pass filter (1 MHz) was used to increase the reliability of triggering on signal bursts and when the room lights were extinguished,* the validated data rate from the ARO model 8 processor (3% window) was approximately 1 per 3 sec. The Doppler frequency was slightly less than 1 MHz. The level

*The signal levels were sufficiently low that room light was the predominant source and neither type of processor worked properly with them on (mean photon count ~ 100 times higher with room lights).

of turbulence was approximately 7-8% as measured by the ARO Model 8 at P_1 = 1.7 watts.

The demonstration of concept feasibility consisted of obtaining mean velocity measurements with the laser power turned down to 540 mw and 100 mw (corresponding to mean photo electron rates of 547 KHz and 105 KHz.) Under the former condition, 1 validated Model 8 measurement was obtained in 30 sec. and at 100 mw, none were obtained in 2 minutes of waiting and twiddling with the trigger threshold. The photon processor was able to make a mean velocity estimate at both 100 mw and 500 mw by operating it in a feedback control loop mode with a human operator adjusting the Wavetek oscillator over a period of a few seconds while watching the accumulator display lights.

5.3.2 Statistical Error

A bias error occurs when the long term average value of a measurement differs from the true average of the quantity being measured. The signal levels were so low that insufficient data was collected to establish very accurate long time averages for either the Model 8 processor data or the photon processor. Also, there is no reason that the ARO processor was exactly correct (3% error window, and very low signal levels). In spite of the above, we have compared the 30 sec (10 measurement) average velocity obtained from the ARO Model 8 at 1.7 watts of laser power with the values obtained by human feedback adjustment of the variable oscillator. The values agree within 4% for the 540 mw case and within 20% for the 100 mw case.

A much better statistical measure of the variability error was obtained for comparison with theory. With the oscillator frequency set at the value which nulled the accumulator, a series of 10 one-second measurements were

made for each laser power level. The value accumulated each time was recorded, and the sample rms deviation was computed as shown in Table 7.

Section 6.0 provides a theoretical equation for the rms deviation of the accumulator results as follows:

$$\sigma = \sqrt{2N} \langle\lambda\rangle \Delta\tau \qquad (5.2)$$

$N = T/\Delta\tau$ is the total number of clock periods during the measurement time. This simplified theory assumes a constant amplitude light source and is therefore only approximate. We have obtained the following comparisons:

P_1	σ Theory	$\hat{\sigma}$ Experiment
100 mw	50.2	48.4
500 mw	285	309.0

Table 7. Comparison of Theoretical and Experimental Standard Deviation of Accumulator Values.

5.4 COUNTER BIAS AND PHOTON CORRELATION

When the feasibility demonstration experiment just described was performed, there were several minor operational problems such as overheating and occasional intermittent accumulator operation which occurred at clock frequencies higher than those required for the demonstration. These problems were fixed later by minor circuit changes and the addition of more powerful cooling fans. On October 10 and 13, 1975 SAI and GW Electronics personnel performed additional laboratory measurements to verify proper operation of all system functions at speeds up to the guaranteed minimum clock frequency of 40 MHz. Two significant additional

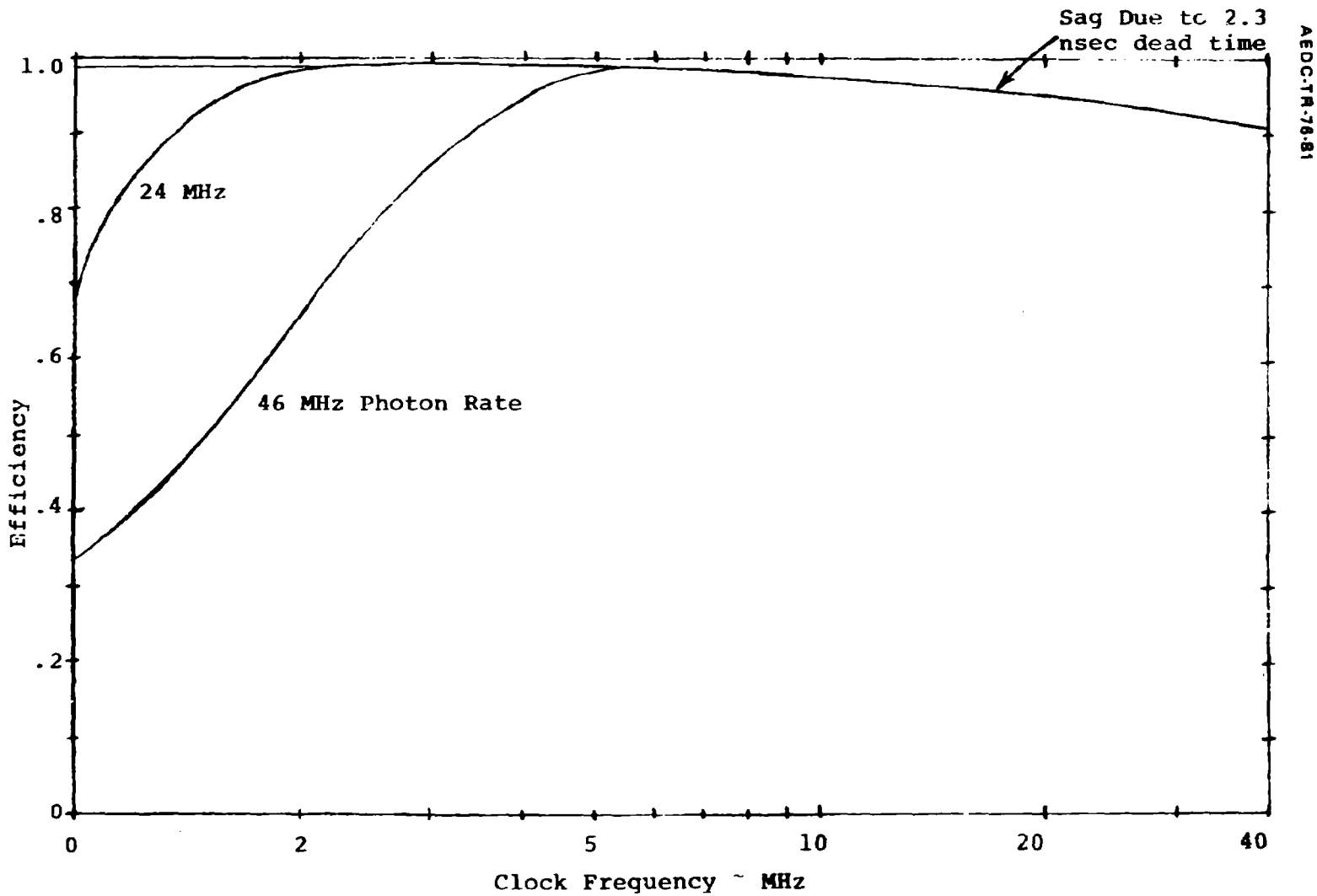

Figure 12. Efficiency of Four-Bit Counter Vs. Clock Frequency and Data Rate.

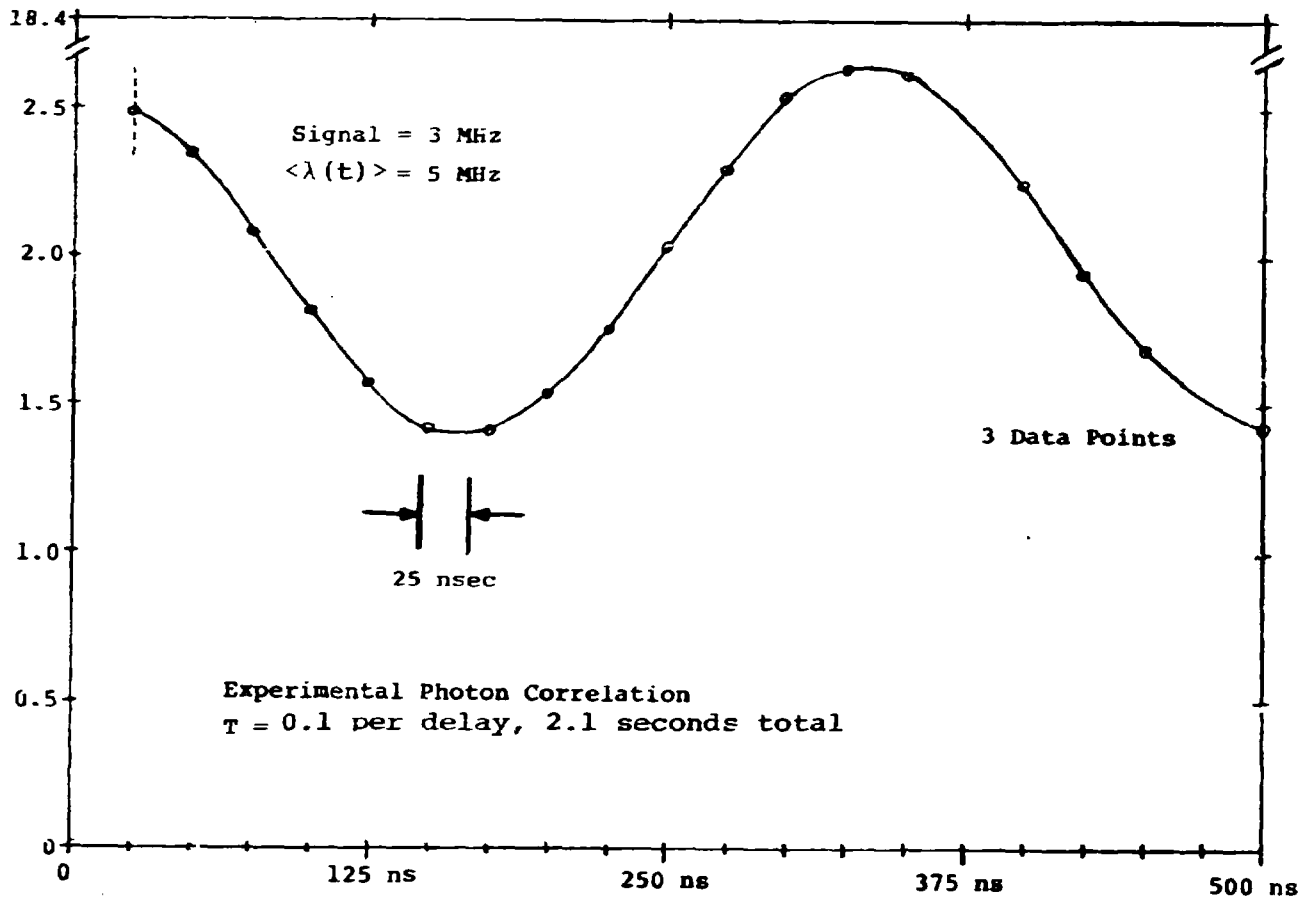

Figure 13. Experimental Photon Correlation.

measurements were conducted using an RCA 8645 PMT with the ORTEC 9301 preamp, and a light emitting diode source (LED).

5.4.1 Counter Bias Vs. Clock Frequency

The design of the 4-bit counter circuit uses two alternating counters with a small dead time between count intervals. In order to measure this effect we placed the processor in MEAN mode, so that it merely accumulated the sum of all the n_k during the counting interval, and compared the sum with the total accumulated by the Systron Donner laboratory counter (SDC) during the same interval. We did this for several different mean photoelectron rates and several different system clock frequencies and parametrically plotted the ratio of the processor total to the SDC total. This data is illustrated in Figure 12. The figure reveals three significant effects upon close scrutiny. First, over most of the data, the count efficiency is not a function of photon rate. Second, at the very low clock frequencies and high photon rates, the count saturates at 15 (4 bit counter) and data is lost. Third the slight high frequency slump is predicted almost exactly by assuming an interperiod dead time of 2.3 nsec.

5.4.2 Photon Correlation

The LED was modulated at 3.000 MHz with the bias dc level adjusted to give a ratio of the peak-to-peak ac light modulation to steady light ratio* of 0.18. The LED was moved away from the shielded PMT (with pinhole) until the mean photo-electron count rate was 5×10^6 or 1.67 photoelectrons per cycle. The photon processor was sequentially

*As measured by an oscilloscope observation of a relatively high level signal output from the PMT directly to a load resistor.

programmed through all delay values with the processor in AUTOCORRELATE MODE, the system clock at 40,00 MHz, and the measurement interval per delay of 0.1 sec. The total photoelectron count was measured by the SDC simultaneously for each delay value. Since the mean photoelectron rate drifted during the time the data were collected, the autocorrelation results were normalized by dividing by the square of the totalized photoelectron count for each delay interval.

The results of this experiment are plotted in Figure 13. It is significant that with an average of 1.7 photoelectronic/cycle, the entire measurement would have required only 2.0 seconds if it had been sequenced by a computer. The value plotted at 500 nsec delay is actually 3 separate 0.1 sec runs. This is an indication of the low variability error for this particular experiment.

6.0 DISCUSSION

In this section we discuss photomultiplier tube effects, burst counter threshold, and errors in the measurement of mean flow with the new Dual Correlate and Subtract technique.

6.1 PHOTOMULTIPLIER TUBE NOISE EFFECTS

There have been so many written statements to the effect that photomultiplier tubes are "nearly noiseless" that we may begin to believe it doesn't matter much which tube is used except for speed, size, ruggedness, quantum efficiency, and cost. For all low level LV signal detection schemes for photon-limited and photon-resolved signals nothing could be less true. The significant factors in addition to the above mentioned are dynode collection efficiency, dynode pulse charge gain statistics, pulse transients (ringing), correlated after pulsing, and total dynode gain. The effects of pulse gain statistics and dynode collection efficiency may be serious even for signals in the Gaussian regime since they may easily reduce the signal power to noise ratio (see equation 2.13 for definition) by a factor of 4 or more. References [16-18] should be read for thorough discussion of effects to be considered. In light of the following, we recommend that the newer tubes with small pulse height variation and high collection efficiency be used in future LV systems.

6.1.1 Dynode Collection Efficiency

The effective quantum efficiency η for photon counting is the product of η_c, the cathode efficiency usually considered

and F, the dynode pulse efficiency. This dynode efficiency F is less than unity because some of the cathode photoelectrons are collected by the dynodes without producing an output pulse. The point missed by many investigators is that the product $\eta_c F$ is the correct quantity to use in SNR equations (or in the computation of $\lambda(t)$) even at high signal levels. It is not difficult to measure η_c by direct cathode sensitivity measurements. The quantity F is not specified in typical manufacturers specifications. Our experience (see Section 5.1.1) is that η may be less than half of the specified quantum efficiency due to either cathode fatigue and/or poor dynode collection efficiency.

6.1.2 Single Photoelectron Gain Variation

The charge delivered to the anode by the ith photoelectron pulse is $e\,g_i$, where g_i is the random charge gain. The relationship between the DC current gain G for a given tube and the average value $\langle g_i \rangle$ of the single photoelectron pulse gain may be shown to be

$$\langle g_i \rangle F = G \tag{6.1}$$

The shape of probability density for g_i determines several significant things including the value of the premultiplier term in the signal-to-noise ratio equation 2.13. Reference [14] pages 65 and 66 would imply that for a typical copper berylium dynode tube with stage gains of 3-4 the reduction factor $\langle g \rangle^2 / \langle g^2 \rangle$ will be in the range 0.5 to 0.76. This is not an insignificant factor and should be included carefully in PMT selection. For some of the newer tubes with high first-stage gain, the factor would be nearly unity.

For very low-level signal detection and photon counting, the pulse height variation is harmful in several ways. First, the variation of height can cause false triggering on the anomalously large pulses in a low-level burst-counter or transient recorder system. In a photon counting system a timing error occurs because of threshold crossing at different portions of the pulse waveform. Another consideration is the fact that for a low-gain PMT the Gaussian electronic preamplifier noise may easily be the same order of magnitude as the smaller single photoelectron pulses. This is true, for example, with the RCA 8644 or 8645 tubes. Another problem with large pulse height variation is that in very fast system, the pulses have a ringing tail no matter how careful we are in the physical arrangement. When we set a discriminator threshold above the ringing tail of the larger pulses, we then miss the smaller ones. Photon counting systems thus need great care in circuit design and construction details and a tube with small pulse height variation.

6.2 BURST HEIGHT DISTRIBUTION EFFECTS

It is clear from the experimental data shown in Figure 11 on burst amplitude vs. rate of occurrence that with natural aerosols there may be a few large signals with adequate "signal-to-noise-ratio" for burst-counter operation and many smaller bursts which produce only a few photoelectron pulses. There are the questions of how do we compare a photon counter processor and a burst counter processor, how do we determine the source distribution of the signals which are rejected by each type of processor and which are accepted.

Appendix B addresses itself to the above questions and produces some answers and some more questions. For example, neglecting PMT pulse pile up and discriminator saturation and dead time effects, the appendix shows that for the experimental data, the slope of the amplitude rate distribution is sufficiently steep that the accumulator sum places emphasis on the smaller scatterers, which produce fewer photons. The appendix does not answer the question of what happens to a photon counting processor when the burst is photon limited and not large enough to go above the discriminator threshold and stay (in which case it would contribute negligibly to the result.) We expect a phase reversal contribution in some cases where the valleys of the signal produce threshold crossings by single photo-electron pulses while the peaks remain above threshold and produce no pulses. For cases where the rate amplitude distribution has sufficiently negative slope in the photon-limited regimes and below, we would expect the as yet unpredictable effects to be negligible in the sum, but obviously further work is needed.

In contrast to the maximum photoelectron rate which a photon counting system can utilize due to electronic limitations, the required rate appears to be much less. The scaled data in Figure 11 indicates a data rate of approximately 100,000 signal burst/sec at the peak rate level of $\geq 10^7$ photo-electrons/second. Since the scaled burst duration is 1 μsecond, this corresponds to a duty factor of 0.1 at this level. These figures are similar to the parameter values chosen in our "typical" variability error example in section 6.3 where the preliminary theory indicates 1% rms variability error in mean flow measurement with 0.5 seconds of data. Our present analysis indicates that with the example optical system the contributing particle size would be primarily in the 0.2 - 0.3μ particle size range.

The lower threshold of burst counter processors is shown as approximately 4 mv or 8 x 10^8 photoelectron pulses sec peak pedastal in Figure 11. This threshold was originally arbitrarily based on the assumption of needing 4 photoelectrons/cycle at the $1/e^2$ pedastal locations with a 25 MHz signal; i.e. we assumed the need for greater than 4 photoelectron pulses/cycle over the $1/e^2$ burst width. This leads to a peak pedastal value of $\lambda_j = e^2 \times 10^8 = 7.4 \times 10^8$.

Independently of the above assumptions, Franz Durst and others in discussions at the 1975 Minnesota Conference [19] indicated that the lower limit of reliable burst-counter operation was at average signal-to-noise power (during peak signal) ratios of 10. From equation 2.13 with 0.707 assumed for $\langle g_i \rangle^2 / \langle g_i^2 \rangle$, we would obtain a requirement for $\lambda_j = 10 \times \sqrt{2} = 14.1$ as a threshold. This would indicate approximately 7-8 mv pedastal signals for the RCA 8644 tube used would be required and our scaled estimate of 300 acceptable burst/sec as too high.

In reality, there is no absolute "threshold" for acceptable burst counter operation. The probability of correct detection is a continuous function of signal amplitude, background level, and low-level signal distribution. The problem of analysis for burst counters is formulated in more detail in Appendix B, but no attempt at its solution is presented. Further work in this area both analytically with simulation is recommended.

6.3 STATISTICAL ERRORS

The two principle types of error which arise in statistical measurements are bias error and variability error. Bias error is a term which refers to the difference between the statistical expectation of the measurement system output and the desired average value being measured. The variability

error is the rms value of the random deviation of a specific experimental result from the statistically expected value. For ergodic random processes, the variability error converges to zero in the limit of infinitely long data collection time; but it converges to an acceptable level (which must be defined in the measurement objectives) within a finite measurement time. The bias error cannot be removed by further averaging but it can often be removed by analytical compensation or by experimental calibration when it is small compared with the desired quantity. In general, analysis of both types of errors is required in any statistical measurement. Bias errors are evaluated by using more precise signal and system models in determining expected values of the output.

Error-analysis of a Dual Correlate and Subtract processor will be presented in more detail in the final report for Contract NASA1-13737, between NASA Langley Research Center and Science Applications, Inc., which is not yet complete. In this section we briefly indicate the nature of bias errors which must be investigated and summarize preliminary variability error analysis results which have been obtained for NASA.

6.3.1 Bias Errors

There are several potential sources of bias error for the processor we have designed. First, the value of n_k does not represent the number of photoelectrons detected at time $k\Delta\tau$. The detection events occur in the time interval $(k-1)\Delta\tau<t<k\Delta\tau$. The effect of this time discretization is similar to that of our previous work [20] in that the expected value of an autocorrelation estimate at a discrete delay is a weighted average of the true autocorrelation function over an interval about that point. The weighting function is

triangular, extending $\pm\Delta\tau$, as is shown in equation 2.24. The effect of a triangular weighting function on the correlation estimate is that of a $[\sin(\pi\Delta\tau f)/\pi\Delta\tau f]^2$ low-pass filter. For $\Delta\tau = 1/4f_m$ the cosinusoidal portion of the autocorrelation estimate is thus attenuated by a factor of 0.81 and lower signal frequencies are attenuated less than higher ones. A small bias of the mean frequency estimate will thus be developed which vanishes for small turbulence intensities or for smaller values of $\Delta\tau$.

Additional bias error will be induced by time jitter in the detection of photoelectron pulses. For a fixed threshold trigger circuit, different portions of the pulse leading edge will trigger the discriminator if the amplitude of the single photoelectron pulses varies. With the presently available PMT's, this jitter can be no more than the rise time of less than 2 nsec but can be reduced to a fraction of a nsec with newer tubes with small pulse height variation. The effect is small compared with the $\Delta\tau$ effect even at the fastest range of 10 nsec.

The threshold discriminator dead time will produce bias errors. It is obvious that if the dead time were 20 nsec, there would be no lag products at a 10 nsec delay interval. The functional dependence of the bias error has not been derived for this system yet. On the highest range, with $\Delta\tau$ = 10 nsec, signal frequency = 25 MHz and with a dead time of 9 nsec, the estimate will be distorted because delay 1 implies events in the range (0.0 $\Delta\tau$, 2.0 $\Delta\tau$) while delay 3 refers to events separated in time by (2.0 $\Delta\tau$, 4.0$\Delta\tau$). Clearly, the delay equal 1 term will be reduced appreciably on the faster ranges. This effect may be seen in Figure 13 where the first delay term appears slightly low. It is possible that correction curves may be derived in conjunction with experimental calibration results, but further work is needed to assess the limitations.

In the hardware design we have included a provision for changing the relative width of $\Delta\tau$ with respect to the signal frequency. This may be accomplished simply by increasing the numbers of clock delays for the indices p and q while keeping their ratios constant. For example, with $\Delta\tau$ = 1/4 period in the dual correlate mode, p = 3, q = 1; by changing p = 6, q = 2 $\Delta\tau$ becomes 1/8 period at the mean signal frequency. The price for the change is the reduction of the maximum potential signal frequency from 25 MHz to 12.5 MHz and increased variability error, but bias error effects due to $\Delta\tau$ width, after-pulse correlation, and discriminator dead time may all be significantly reduced.

The analytical formula for the statistical expectation of the output of a photon correlator was obtained using 3.7:

$$\langle \cos \omega_j \tau \rangle = \int_{-\infty}^{\infty} p_\omega(\omega) \cos \omega\tau \, d\omega = e^{-\frac{\tau^2 \sigma_\omega^2}{2}} \cos \omega_m \tau \quad (6.3)$$

The specific result depended on both the assumption that $p_u(u)$ was Gaussian and the assumption that particle rate bias effects did not keep $p_\omega(\omega)$ from being the same shape. It is not difficult to show that cos $\omega_m\tau$ factor will always result if $p(\omega)$ is symmetrical about its mean ω_m. The question of concern is "what happens if $p(\omega)$ is skewed?" Preliminary efforts indicate that there are error contributions from higher order odd central moments of $p(\omega)$, whose magnitude depends on the deviation of the discriminator characteristic from linearity and which vanish with decreasing turbulence intensity as expected. This work has not been refined to the point of formal reporting. We feel intuitively that the results will show that the problem is minor for turbulence levels on the order of 10% or less. For

higher turbulence levels, up shifting with a Bragg cell or other means may be required to keep $p(\omega)$ confined to the linear region of the discriminator function. It may also be possible in further work to identify configurations for which the discriminator characteristic is more linear.

6.3.2 Variability Error

In an earlier very brief contract with NASA Langley (NAS1-13140) a simplified variability error analysis was performed on the accumulator sum under the assumption that the classical optical power was steady at its mean value. In that case analysis of the variance led to the simple rms result:

$$\sigma_{\hat{m}pq} = \sqrt{2N}\ \langle\lambda\rangle\ \Delta\tau \tag{6.4}$$

which although much oversimplified has shown good agreement with experiment (see Section 5.3.2). In the rest of this subsection we paraphrase the NASA1-13140 report* in which we applied equation 6.4 to obtain an estimate of the fractional rms velocity error, $\varepsilon_u = \sigma_u / \bar{U}$. The resulting approximation was

$$\varepsilon_u \approx \frac{2\left[\frac{\lambda_b}{\lambda_s} + 1\right]}{\pi\ \lambda_a\ \sqrt{T\Delta\tau}} \tag{6.5}$$

where

$$\lambda_b = \text{background photoelectron rate} \tag{6.6}$$

λ_s = mean signal rate = $R\langle\lambda_j\rangle\sqrt{\pi}\ \alpha$

$\lambda_a = \langle\lambda_j\rangle$ = mean peak pedastal photoelectron rate

$T = N\Delta\tau$ = data collection time

*Interim project report; not distributed

In order to provide further intuitive insight concerning equation 6.5 we include the following example numbers which might be typical for a transonic measurement:

$$\lambda_b = 10^7/\text{sec} \qquad (6.7)$$
$$\lambda_s = 10^6/\text{sec}$$
$$\lambda_a = 10^7/\text{sec}$$
$$\Delta\tau = 10^{-8}\ \text{sec}$$
$$\varepsilon_u = 0.01$$
$$T = 0.49\ \text{sec}$$

In this example, the mean signal photoelectron rate is ten times less than the mean background photo-electron rate and is equal to the average peak envelope rate. With this much background light, the assumption of constant P(t) is valid with respect to the photon-fluctuation induced variability. The selection of mean peak rate at 10^7 means that occurrences of photoelectron count rates greater than 10^8/sec (the limit of current hardware state of the art) will be rare and the effects of nonlinearity negligible). The selected ratio of $\lambda_a/\lambda_s = 10$ implies that the measurement volume is only assumed to contain a scatterer 1/10 of the time on the average.

Even though dramatic improvements over the previous example situation may result from reduced background light, the result still indicates that practical measurements may be obtained with a peak signal photoelectron rate of 10^7/sec. In order to compare this with the performance of a burst-counter system, we must assume values for p, q and f_m, the Doppler frequency. With p = 3, and q = 1 the Doppler frequency f_m is $1/4\Delta\tau = 25$ MHz. This would result from $\bar{U} = 1000$ ft/sec with an optical sensitivity of 25 KHz/ft/sec. This peak photoelectron rate assumed is thus 0.4 photoelectrons/

cycle in the presence of 0.4 background photoelectrons/cycle. For comparison we note that the signal-to-noise ratio formula of equation 2.14, given $\eta P(t)/h\nu = \lambda_a (1 + \cos \omega_m t) + \lambda_b$, would result in peak average SNR (using $2B = 1/\Delta\tau$) of

$$SNR = \frac{\lambda_a^2}{4B(\lambda_a + \lambda_b)} \tag{6.8}$$

In our example, B = 25 MHz and $\lambda_b = 10^7$; if we choose $\lambda_a = 10^9$, a factor of 100 greater than in our example, then the SNR is 10 at the peak of the signal burst and 1.35 at the 1/e signal envelope points. Since this example represents marginal or inadequate SNR for burst counter operation we deduce that, even with 100 times more scattered power, only the larger-than-average scatterers would contribute.

Under conditions of less background light, the burst-counter analysis would not be improved; however, the photon counting system results are expected to improve considerably. Thus we conclude that mean-flow measurements with from 100 - 1000 times less optical power are feasible with the photon counting system.

7.0 CONCLUSIONS

The effort under this contract has resulted in several significant conclusions both theoretical and experimental. These are summarized below.

Theoretical Poisson models have been formulated for dual-scatter LV signals with sufficient generality to include all signal regimes from classical signals with Gaussian noise down to photon-resolved signals which require photon counting techniques.

Analysis of conditional signal models has provided instantaneous signal-to-noise ratio and other statistical parameter equations not previously available in the LDV literature.

Analysis of Unconditional models has indicated the practical feasibility of improving detection sensitivity over burst-counter techniques by a factor between 100 and 1000 by using photon counting techniques.

A detailed analysis, including explicit mention of approximations required, of the expected value of direct photon correlation of LV signals from turbulent flow is provided. This both supports and points out limitations of previous results given by Pike and others.

A new Dual-Correlate-and-Subtract technique for new frequency measurement which utilizes only two delay values and one real-time high speed multiplier without clipping has been theoretically shown to be feasible. This feasibility is based on evaluation of the expectation for system model to show convergence to mean frequency estimate, and on rms variability analysis which indicates practical measurement times on the order of 0.5 seconds in transonic flow.

An electronically switchable, multipurpose, high-speed electronic signal processor with the potential speed for 10 nsec time resolution and 10 nsec real time 4 bit multiplication

has been designed and constructed using slow ECL integrated circuits on special-purpose 100 MHz wirewrap panel. The system implements the dual-correlate-and-subtract technique. It also has the potential of standard photon correlation without clipping by computer controlled scanning of the delays. The computer interface has not yet been constructed however. If the computer interface is developed, the system will also be capable of measuring multipoint statistics of any high-speed events (up to 100 MHz).

Experimental measurements have been performed which verify the operation of the photon processor with 100 MHz input events and 40 MHz system clock operating speed. A sequential photon correlation of a low-level sinusoidally modulated optical source has been made with 25 nsec time resolution. The mean velocity of a low-speed jet was measured with the dual correlate of subtract mode under conditions for which no burst counter data could be obtained.

Photon counting experimental work requires much more care in selection and use of photomultiplier tube components than does burst-counter work. However, single photoelectron pulse height statistics and dynode collection efficiency can easily reduce the effective signal power to noise power ratio by a factor of 4 for two tubes with the same quantum efficiency. This can significantly effect a burst counter system sensitivity.

The statistical distribution of the amplitudes and rates of occurrence of classical bursts has been shown to be central in the problem of specifying or predicting the data rates and errors from any type of LV signal processor. Differential and cumulative rate/amplitude distributions have been formulated and analyzed theoretically and have been measured experimentally for an argon backscatter LV system. The results indicate that, for the data obtained, the smaller aerosols contribute more to the photon correlation accumulator than the larger ones. For the data measured, there would have been available less

than 300 signals per second adequate in magnitude to produce burst counter data from scatterers larger than 0.7 micron in diameter while there would have been over 100,000 signals per second producing photon resolved signals from 0.2 - 0.3 micron diameter particles.

We have demonstrated both theoretically and experimentally that there are LV signals that require the use of photon counting techniques; and we have delivered a new type of photon counting instrument which will potentially operate to 10 nsec time resolution with full 4 bit multiplication.

Further effort with computer controlled data collection is required to explore the potential of the new system and fully define its limitations.

REFERENCES

1. Mayo, W. T., Jr., Laser Doppler Flowmeters - A Spectral Analysis. Ph.D. Thesis, Georgia Institute of Technology. Atlanta, Georgia, May, 1969.

2. Allen, J. B., Estimation of the Frequency of Laser Velocimeter Signals. Ph.D. Thesis, Georgia Institute of Technology. January, 1973.

3. Durrani, T. S., Noise Analysis for Laser Doppler Velocimeter Systems. IEEE Transactions. COM-20: 296-307. 1973 (June). See also Durrani, T. S., and Greated, C. A., Statistical Analysis and Computer Simulation of Laser Doppler Velocimeter Systems. IEEE Transactions. IM-22: 23-34. 1973 (March).

4. Meyers, J. F., Computer Simulation of a Fringe Type Laser Velocimeter. In: Proceedings of the Second International Workshop on Laser Velocimetry, Purdue University, March 27-29, 1974.

5. George, W. K. and Lumley, J. L., The Laser Velocimeter and its Applications to the Measurement of Turbulence. Journal of Fluid Mechanics. 60, pt. 2: 321-362, 1973.

6. Snyder, D. L., Random Point Processes. New York, John Wiley and Sons, Inc., 1975. (Schedule for publication September).

7. Papoulis, A., Probability, Random Variables and Stochastic Processes. New York, McGraw-Hill. 1965.

8. H. Z. Cummins and E. R. Pike, Editors, Photon Correlation and Light Beating Spectroscopy, NATO Advanced Study Institute Series, Plenum Press, New York, 1974.

9. E. R. Pike, The Application of Photon-Correlation Spectroscopy to Laser Doppler Velocimeter, The Use of the Laser Doppler Velocimeter for Flow Measurements, Proceedings of a workshop, Purdue University, LaFayette, Indiana, March 1972.

10. W. T. Mayo, Jr., Modeling Laser Velocimeter Signals as Triply Stochastic Poisson Processes, in the Proceedings of the Minnesota Symposium on Laser Doppler, University of Minnesota, Bloomington MI, October 1975.

11. E. V. Hoversten, D. L. Snyder, R. O. Harger, and K. Kurimoto, Direct Detection Optical Communication Receivers, IEEE Trans. on Communications, COM-22, No. 1, 17 (January, 1974).

12. Farmer, W. M., The Interferometric Observation of Dynamic Particle Size Velocity, and Number Density, Ph.D. Dissertation, The University of Tennessee. 1973.

13. Bertolotti, M., Photon Statistics, In: Photon Correlation and Light Beating Spectroscopy, H. Z. Cummings and E. R. Pike (ed.) New York, Plenum Press 1974.

14. R.C.A. Photomultiplier Tube Manual, Technical Series PT-61, RCA Electronic Components, Harrison, N.J. 07029 (1970).

15. A. D. Birch, D. R. Brown, J. R. Thomas, and E. R. Pike, The Application of Photon-Correlation Spectroscopy to the Measurement of Turbulent Flows, J. of Physics D: Applied Physics, 6, L71, (1973).

16. R. Foord, R. Jones, C. J. Oliver, and E. R. Pike, The Use of Photomultiplier Tubes for Photon Counting, Applied Optics, 8, No. 10, p. 1975 (October, 1969).

17. R. Jones, C. J. Oliver, and E. R. Pike, Experimental and Theoretical Comparison of Photon-Counting and Current Measurements of Light Intensity, Applied Optics, 10, No. 7, 1673 (July 1971).

18. A. T. Young, Use of Photomultiplier Tubes for Photon Counting, A Letter to Applied Optics, 10, p. 1681 and Author's Reply, same issue, p. 1683 (July 1971).

19. University of Minnesota Symposium on Laser Doppler Anemometry, Bloomington, Minnesota, October 22-24, 1975.

20. W. T. Mayo, Jr., M. T. Shay, and S. Riter, The Development of New Digital Data Processing Techniques for Turbulence Measurements with a Laser Velocimeter, Final report (AEDC-TR-74-53), USAF Contract No. F40600-73-C-003, August 1974.

21. H. C. Van De Hulst, Light Scattering by Small Particles, John Wiley & Son, New York, N.Y., 1957.

APPENDIX A

FILTERED INHOMOGENEOUS POISSON PROCESSES

In this appendix we have provided introductory background theory for filtered inhomogeneous Poisson processes. For more introduction, the reader is referred to Papoulis [7] or to the more advanced text by Snyder [6].

A.1 INHOMOGENEOUS POISSON IMPULSE PROCESSES

The input to a random linear system is a inhomogeneous Poisson impulse process z(t) given by

$$z(t) = \sum_{-\infty}^{\infty} \delta(t - \tau_i) \tag{A.1}$$

where $\{\tau_i\}$ is the set of random occurrence times, $\lambda(t)$ is the instantaneous statistical mean value of z(t), (and also the mean rate of occurrence of the τ_i's), and $\delta(t)$ is the dirac delta function. The random variables τ_i are independent of each other statistically and obey the inhomogeneous counting law, i.e., the probability of n = k occurrences in the interval (t_1, t_2) is

$$P\{n(t_1,t_2) = k\} = \frac{e^{-\mu}(\mu)^k}{k!} \tag{A.2}$$

where

$$\mu = \int_{t_1}^{t_2} \lambda(t)dt \tag{A.3}$$

The quantity μ is also the mean and variance of the random variable $n(t_1,t_2)$.

A.2 THE RESPONSE OF A RANDOM LINEAR SYSTEM-CAMPBELL'S THEOREM

The output of the random linear system $s(t)$ is the superposition of the response $h(t-\tau_i, \bar{Y}_i)$ to each input impulse:

$$s(t) = \sum_{-\infty}^{\infty} h(t-\tau_i, \bar{Y}_i) \qquad (A.4)$$

where $\{\bar{Y}_i\}$ is a set of identically distributed, independent, vector random variables. The random variable $\bar{Y}$ affects the shape and amplitude of the response function $h(t,\bar{Y})$. In the case of the PMT signal it may take the form of a single scalar amplitude variable. In the case of the classical optical signal from turbulent flow both a random amplitude parameter and one or more random shape parameters due to velocity magnitude, direction, and probe volume translational entrance location may be required. The theory should be applicable so long as the set of multidimensional random variables $\bar{Y}_i$ is independent of the set of occurrence times $\{\tau_i\}$. The generalized Campbell's theorem results for the instantaneous statistical mean, variance, and auto-covariance of $s(t)$ are given below, they apply regardless of whether individual pulses are resolved or not.

$$\langle s(t)\rangle = \int_{-\infty}^{\infty} \lambda(\tau)\langle h(t-\tau, \bar{Y}\rangle d\tau \qquad (A.5)$$

$$\sigma_s^2(t) = \langle s^2(t)\rangle - \langle s(t)\rangle^2 = \int_{-\infty}^{\infty} \lambda(\tau)\langle h^2(t-\tau,\bar{Y})\rangle d\tau \qquad (A.6)$$

$$\text{cov } s(t_1)s(t_2) = \langle s(t_1)s(t_2)\rangle - \langle s(t_1)\rangle\langle s(t_2)\rangle \qquad (A.7)$$

$$= \int_{-\infty}^{\infty} \lambda(\tau)\langle h(t_1 - \tau, \bar{Y})h(t_2 - \tau, \bar{Y})\rangle d\tau$$

where < > denotes expectation with respect to $\bar{Y}$ inside the integral signs. For a causal signal such as that from the PMT, where h(t) is zero for $t \leq 0$, the the upper limits of integration may be replaced by t or the minimum of t_1 and t_2 in equation (A.7). For the transient case where the impulse signal z(t) is applied at t = 0, the lower limits of integration may be replaced by 0.

APPENDIX B

CAUSES AND EFFECTS OF THE DISTRIBUTION OF CLASSICAL SIGNAL BURST AMPLITUDES

The second phase of this contract was an attempt to experimentally and theoretically describe the statistics of signal burst rate and amplitude and relate these to the particle size distribution, the optical parameters, and the electronic parameters in a manner which would ultimately allow prediction of behavior of both photon counting and burst counter data processing electronics.

We accomplished our objectives for some specialized cases of small particles in the submicron size range and somewhat specialized optical geometry. We defined rate and amplitude functions which should be studied further, and we developed the theory enough to conclude that with data such as are obtained experimentally (argon backscatter) the primary contributors to photon correlation were the smaller amplitude signals. The following material is reproduced with heading and reference changes from our Second Interim Report (an unpublished document) without further refinement of the theory.

B.1 RATE AND AMPLITUDE DISTRIBUTIONS OF THE CLASSICAL SIGNAL

In this Appendix we are concerned with the probability density for the signal burst amplitude λ_j, the rate of burst occurrence R(t) and additional rate/amplitude distributions which will be defined. These distributions are essential in statistically relating an accumulated average LV measurement result to the size of the particles which contributed to the

result, to the data rates, the processor efficiency, bias errors, and other quantities of interest. We are not aware of any previous efforts of this type.

B.1.1 The Optical Response Function

We restrict the velocity field to small turbulence with the mean flow in the $\underline{a}_x$ direction normal to the fringes of a one-component dual scatter-system. Off-axis collecting optics with a rectangular spatial filter are placed either with the optical axis in the plane of the two matched transmitter beams (case 1) or in the normal plane which includes the bisector (z axis) of the transmitter beams (case 2). In either case the width of the rectangular aperture in the image plane of the collecting lens is $2cw_o$ where c is a constant and w_o is the $1/e^2$ radius of the transmitted beams in the probe volume. The projection of the length of the rectangular aperture defines the length of the probe volume in the z direction. For case 2 there are no end effects; for case 1, scatterers passing through the ends of the probe volume will produce burst wave forms with one side clipped considerably. The length L_z will be assumed long enough to neglect these end effects, but short enough to maintain high fringe contrast and uniformity of intensity in the z direction. The scatterers are assumed small enough for validity of the fringe model and the assumption of a broad scattering pattern so that perfect signal fringe contrast is obtained. With all these assumptions we may determine the optical power collected at the PMT photocathode from a single scatterer at position (x_j, y_j, z_j) in terms of λ as follows

$$\lambda(x,y,z) \propto \gamma e^{-\frac{2(x^2+y^2)}{w_o^2}} (1 + \cos 2\pi f_x x) \text{ Rect}\left[\frac{\alpha}{2cw_o}\right] \qquad (B.1)$$

when $|z| < L_z/2$, and is zero when $|z| > L_z/2$, where

$\alpha = y$, case 1

$\alpha = x$, case 2

and where

$$f_x = \frac{2}{\lambda_o} \sin \frac{\theta}{2} = \text{fringe period} \qquad \text{(B.2)}$$

$$\gamma = \left(\frac{\eta}{h\nu}\right)\left(\frac{\pi D^2}{4}\right)\eta_T\left(\frac{i(a)\lambda_o^2}{(2\pi F)^2}\right)\left(\frac{2P_L}{\pi w_o^2}\right)$$

D = collecting lens diameter

T = combined transmission efficiency of transmitter and receiver optics including any spectral filter.

λ_o = optical wavelength

F = focal length of collecting lens

P_L = total laser power

$i(a)$ = scattering coefficient (Van deHulst)[21]

The expression for γ is broken down in parentheses to sequentially show the effects at the PMT cathode, the collecting lens area, the scattered intensity, and the incident power density at the center of the probe volume (excluding fringe variation from pedastal.) The Rect function shows the effect of the width of the spatial filter aperture. The Mie scattering coefficient defined by Van DeHulst as a function of a, the particle radius, is selected as $i_{\parallel}$ or $i_{\perp}$ depending on whether the (linear) polarization of the incident light is parallel or perpendicular the plane of scattering.

We now assume that the jth scatterer passes the yz plane at time τ_j, and at location (y_j, z_j) with velocity $U\underline{a}_x$ and scattering coefficient $i(a_j)$. This results in the time response

$$\lambda_j(t) = \lambda_j \text{ Rect}[\alpha/2cw_o] \text{ Rect}[z_j/L_z] \qquad (B.3)$$

$$e^{-2[(t-\tau_j)U]^2/w_o^2}[1 + \cos(2\pi f_x(t - \tau_j)U]$$

$\alpha = y_j$, case 1

$\alpha = (t - \tau_j)U$, case 2

where

$$\lambda_j = \gamma(a_j)e^{-2y_j^2/w_o^2} \qquad (B-4)$$

B.1.2 Probability Density of λ_j

The result of equation B.3 is the product of a normalized function displaced in time to $t = \tau_j$ with a random amplitude which is the product of two independent random variables $\gamma_j = \gamma(a_j)$ and Y_j where

$$\gamma_j = f_1(a_j) \qquad (B.5)$$

$$Y_j = f_2(y_j) = \exp[-2y_j^2/w_o^2]\text{Rect}[\frac{\alpha}{2cw_o}]\text{Rect}[\frac{z_j}{L_z}]$$

In a more general model, the signal amplitude would also depend on direction and other position variables (x_j, y_j) and the shape of the normalized function would also depend on these quantities. The purpose of our simplified model is to examine the effect on $p_\lambda(\lambda)$ of the dependence of λ_i on both particle radius and probe volume entrance location. Papoulis [7] gives theory required to obtain density $p_\lambda(\lambda)$ for the product $\gamma_j Y_j = \lambda_j$ in terms of the density $p_\gamma(\gamma)$ and $p_Y(Y)$

$$p_\lambda(\lambda) = \int_{-\infty}^{\infty} \frac{1}{|\alpha|} p_\gamma(\alpha)p_Y(\frac{\lambda}{\alpha})d\alpha \qquad (B.6a)$$

$$= \int_{-\infty}^{\infty} \frac{1}{|\alpha|} p_\gamma(\frac{\lambda}{\alpha})p_Y(\alpha)d\alpha \qquad (B.6b)$$

where in B.6 α is a dummy integration variable. The densities $p_\gamma(\gamma)$ and p_Y are straight-forward in principle to obtain from the particle radius a_j density and the density for the location y_j. Papoulis gives the density for a function of a random variable from which we obtain:

$$p_\gamma(\gamma) = \frac{p_a(a)}{|f_1(a)|} \quad \text{at } a = f_1^{-1}(\gamma) \tag{B.7a}$$

$$p_Y(Y) = \frac{p_y(y)}{|f_2(y)|} \quad \text{at } y = f_2^{-1}(Y) \tag{B.7b}$$

The notation in these formulas means, for example in B.7a, the argument of the density $p_a(a)$ is replaced by the inverse function of γ. This density is divided by the first derivative of the function f_1 (where $\gamma = f_1(a)$) and evaluated at a = inverse function of γ.

When we consider the evaluation of equations B.6 and B.7 even for our simplified model given by equations B.1 through B.5, we see that the relationship of signal amplitude density to particle diameter density is very complex and is not related by a one-to-one function because of the random entrance location multiplier Y. Complete evaluation would require the Mie scattering function, its first derivative, its inverse and the particle size density.

B.1.3 Simplified Evaluation Examples

The nature of the results in equations B.6 and B.7 can be demonstrated by the use of simplified examples. First we consider monosized scatterers and then we consider a rth power law approximation of the Mie scattering function.

B.1.3.1 Monosized Scatterers

With $a = a_o$ for all scatterers, we obtain

$$Y = Y_o \tag{B.8}$$

$$p_Y(Y) = \delta(Y - Y_o)$$

where δ is the dirac delta function. This makes evaluation of equation B.6 simple once we determine $p_Y(Y)$. First consider case 1 where the receiver aperture restricts $|y_i|$ to values less than cw_o. The function $Y(y)$ is even and we obtain correct results by considering the half interval $0 \leq y_i \leq cw_o$. For uniform particle distribution in volume with no velocity gradients, the density for y_i is uniform and given by

$$p_{yi}(y) = \frac{1}{cw_o}, \quad 0 < y < cw_o \tag{B.9}$$

$$= 0, \quad \text{otherwise.}$$

From B.7a and B.5

$$p_Y(Y) = \frac{1}{2\sqrt{2}\ cY\sqrt{-\ln Y}}, \quad e^{-2c^2} < Y \leq 1 \tag{B.10}$$

$$= 0, \quad \text{otherwise}$$

This density is plotted in Figure B1 with $c = 1$ (aperture matched to $1/e^2$ probe width.) The dashed line indicates the shape (values off by $1/\sqrt{2}$) which would result with the aperture matched to the $1/e$ radius $w_o/\sqrt{2}$.

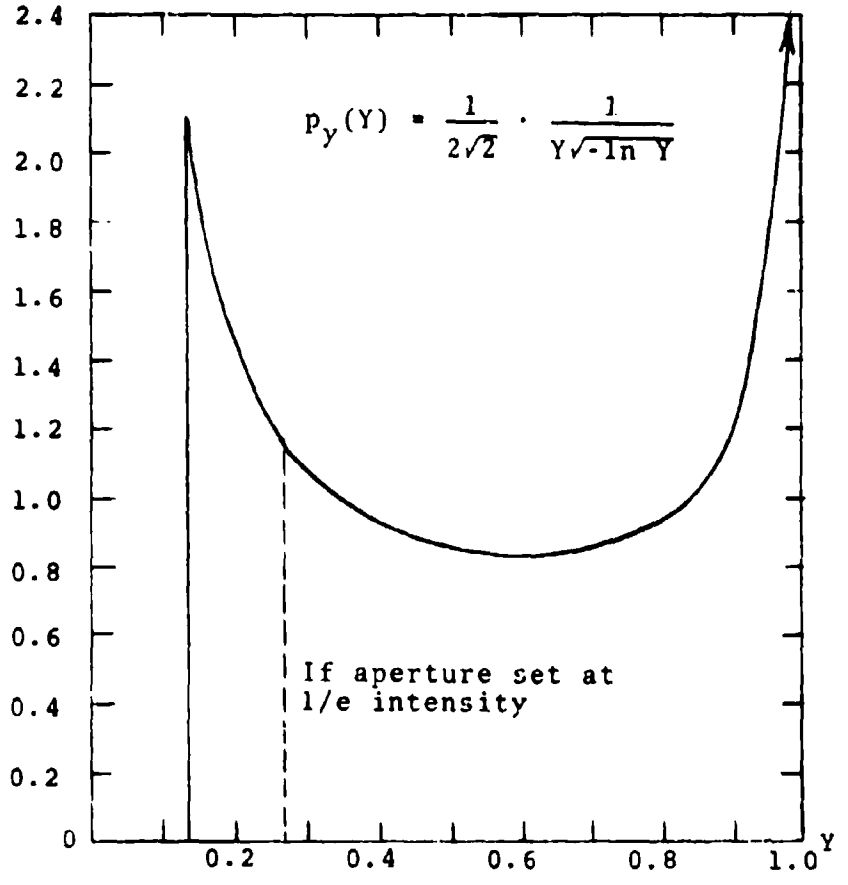

Figure B1. The Probability Density $p_Y(Y)$ for the Random Probe Volume Multiplier.

When equations B.8 and B.10 are substituted into B.6a we obtain the density $p_\lambda(\lambda)$ as

$$p_\lambda(\lambda) = \frac{1}{\gamma_o} p_\gamma\ (\lambda/\gamma_o) \qquad (B.11)$$

$$= \frac{1}{2\sqrt{2}\ c\ \lambda\sqrt{-\ln(\lambda/\gamma_o)}}, \gamma_o e^{-2c^2} < \lambda < \gamma_o$$

In other words, with monosized particles, the density for the burst amplitudes λ_i assumes the shape of the density for the random probe volume multiplier Y. When the case 2 optical system is considered, the result is the same except c is chosen much larger than 1. When this is done the results become singular in the limit of large c. Qualitatively, the result shows large relative probability of λ_i near zero. We will show later how the singularity vanishes in application problems.

B.1.3.2 Power Law Scattering

When the distribution of particle diameter lies entirely in the Rayleigh size regime, then the Mie scattering (equation B.2) behaves as the 6th power of the radius a. In some cases we may approximate the function $\gamma(a)$ as an rth power function over a significant range of values of a so that

$$\gamma(a) = \gamma_o \left(\frac{a}{a_o}\right)^r \qquad (B.12)$$

where γ_o is the value of γ at a selected value of $a = a_o$. Let us assume that in the same range of a, the density $p_a(a)$ for particle radius obeys a qth power law:

$$p_a(a) = p_{ao} \left(\frac{a}{a_o}\right)^q \qquad (B.13)$$

where p_{ao} is a constant. In this case we may evaluate equation B.7a to determine the behavior of $p_\gamma(\gamma)$ in this range. The result is

$$p_\gamma(\gamma) = p_{\gamma o}\left(\frac{\gamma}{\gamma_o}\right)^{(1+q-r)/r} \tag{B.14}$$

where $p_{\gamma o}$ is a constant. As an example, if Rayleigh scatterers ($r = 6$) were distributed with a density behaving as $q = -4$, then the density for γ behaves as $(\gamma/\gamma_o)^{-1.5}$. By comparison, with $r = 4$ and $q = -7$, the density for γ would go as $(\gamma/\gamma_o)^{-2.5}$.

In order to determine the shape density $p_\lambda(\lambda)$, given $p_\gamma(\gamma)$ over a wide of γ, we could again utilize equation B.6. This has not been done at this time. However, the results of the preceding example show that a particle with radius a contributes a value of λ between $e^{-2c^2}\,\gamma(a)$ and $\gamma(a)$. The results of the present example are referred to in later sections.

B.1.4 Burst Rate

B.1.4.1 Introduction. The nature of an LV signal is affected by all of the burst signals present regardless of whether they are of sufficient amplitude to appear as classical signals and/or cross a threshold level. Theoretically we can work with $\lambda(t)$ even in the photon-resolved cases, and must therefore have precise definition of the rate R(t) of occurrence of the bursts in addition to the probability density $p_\lambda(\lambda)$ for their amplitudes. If we were given monosized scatterers with number density ρ (scatterers/m^3) and a sharply defined probe volume cross-sectional area A_v normal to the vector velocity $\bar{V}$ then obviously

$$R(t) = |V(t)|\,\rho\,A_v \tag{B.15}$$

If velocity gradient effects were to be included, a surface integral would replace equation B.15, and the formulation of $\lambda(t)$ as an inhomogeneous filtered Poisson process would have to be extended as a superposition of such processes.

In many practical problems, some of the boundaries of the probe-volume cross-sectional area are not sharply defined and an arbitrary definition (such as the $1/e^2$ intensity contour) is meaningless when a wide distribution of values of γ (particle size) is present. In such cases equation B.15 must be used with definition of ρ and A_v. The cumulative number density of particles with radius a greater than a' is

$$N_a(a > a') = \int_{a'}^{\infty} n_a(a)da \qquad (B.16)$$

and $\rho = N_a(a>o)$ where $n_a(a)$ is a differential size/number density distribution. We observe that $p_a(a)$ and $n_a(a)$ are related by the normalizing constant ρ

$$p_a(a) = \frac{n(a)}{\rho} \qquad (B.17)$$

Thus, the relationship between the cumulative probability function and the cumulative number density function is

$$P(a<a') = 1 - \frac{1}{\rho} N_a(a > a') \qquad (B.18)$$

B.1.4.2 Burst Rate/Amplitude Distribution. When ρ and A_v are well-defined then equation B.15 is applicable. We may also define a differential distribution $r_\lambda(t,\lambda)$ given by

$$r_\lambda(t,\lambda) = R(t)\ p_\lambda(\lambda) \qquad (B.19)$$

The cumulative rate is the integral of this function:

$$R_\lambda(t,\lambda > \lambda') = \int_{\lambda'}^{\infty} r_\lambda(t,\lambda)d\lambda \qquad (B.20)$$

in this definition, $R(t) = R_\lambda(t,\lambda>o)$. The definitions of the rate functions seem redundant. However with extended definition as a limit of a conditional function (Sections B.1.4.3 and equation B.32), there are cases where $r_\lambda(t,\lambda)$ has meaning where $p_\lambda(\lambda)$ does not.

B.1.4.3 Extended Definitions of Number Density and Cross Sectional Area

In practice we must deal with experimental situations where it is not practical to determine the shape of $p_\lambda(\lambda)$ precisely in the range of small values of λ_j. In some such cases, the signal and noise contributions from the small signals may be lumped together approximately as an additional background-light term without significant error, but this is not always true. An approach is needed which allows the analysis to proceed to the point of ascertaining the effects contributed by the small λ tails of the density $p_\lambda(\lambda)$. We find this in the use of conditional densities and rates. We assume that all particle radii "a" are greater than some minimum radius a_1 and that the probe-volume cross-sectional area is limited by sharply defined boundaries in terms of a parameter $\bar{A}$, ("c" in the preceding optical examples). Then we determine $p_\lambda(\lambda|a_1,\bar{A})$, use it in the analysis of the processor behavior to obtain a result, and finally take limits as a_1 goes to zero and the cross sectional area goes to infinity. In the last step, precise models for $p_a(a)$ and the optical response function only become necessary if the final result shows significant changes as the limits are evaluated.

In our case 2 optical example we implicitly demonstrated the approach of finding $p_\lambda(\lambda)$ conditioned on $\bar{c}$. In order to find the conditional density, given that all scatterers are larger in diameter than a_1, we replace $p_a(a)$ in the formulas with $p_a(a|a>a_1)$ given by

$$p_a(a/a > a_1) = \frac{n_a(a)}{N_a(a > a_1)} , \quad a > a_1 \qquad (B.21)$$

$$= 0 \qquad a \leq a_1$$

instead of using (B.17). Similarly, $\rho = N_a(a > o)$ is replaced by $N_a(a > a_1)$ in all formulas. For example, equations B.19 and B.15 become

$$r_\lambda(t,\lambda,a_1,\bar{A}) = R(t|a_1,\bar{A})p_{\lambda j}(\lambda|a_1,\bar{A}) \qquad (B.22)$$

$$R(t|a_1,\bar{A}) = |\bar{V}(t)|\ N_a(a > a_1)A_v(\bar{A}) \qquad (B.23)$$

when the limit of $r_\lambda(t,\lambda,a_1,\bar{A})$ is determined as $a_1 \to 0$ and $A_v \to \infty$ as in equation 4.9, then the function $r_\lambda(t,\lambda)$ which results is well behaved except possibly at $\lambda = 0$, and $R_\lambda(t,\lambda > \lambda')$ is defined for all values of $\lambda' > 0$. Physical reasoning shows that the product $\lambda R(\lambda > \lambda')$ approaches a finite or zero value as $\lambda \to 0$, since this product represents the signal power contained in the low-amplitude bursts.

B.2 APPLICATION TO PHOTON CORRELATION

We are now able to quantitatively describe the expected value of the output of the accumulators in a photon correlation experiment in terms of the system parameters. We also have a way of looking at how the accumulator output is weighted with respect to the distributions of the burst amplitudes.

B.2.1 Expected Accumulator Values

We may rewrite equation 2.6* in conditional notation with

$$\langle n_k | \lambda(t) \rangle \approx \Delta\tau\lambda(k\Delta\tau) \tag{B.24}$$

Following through with $\lambda(t) = \eta P(t)/h\nu$, the expected value of the accumulator sum is

$$\langle A_j \rangle = \left\langle \sum_{k=1}^{N} n_k n_{k+j} \right\rangle = N\langle n_k n_{k+j} \rangle \approx N(\Delta\tau)^2 \langle \lambda(t)\lambda(t+j\Delta\tau) \rangle \tag{B.25}$$

when $j \neq 0$. Equation (2.15)* omitted background light and variation of the shape of the envelope of $f(t)$ with w_i. These effects are now included in equations 3.1 - 3.8, when the rate of occurrence $R(t)$ of the bursts is a constant R. For the case 1 optical model of equation B.3 and B.4

*In this subsection, an asterisk on an equation number refers the reader to Interim Report #1, August, 1974. That report is unpublished, but the material is not necessary here.

with steady x directed flow we obtain:*

$$\langle \lambda(t)\lambda(t+\tau)\rangle = \left(\lambda_b + \frac{\langle \lambda_j \rangle R w_o}{U}\sqrt{\frac{\pi}{2}}\right)^2 \qquad (B.26)$$

$$+ \frac{R\langle \lambda_j^2 \rangle \sqrt{\pi}\, w_o}{2U} e^{-\tau^2 U^2/w_o^2}\left[1 + \frac{1}{2}\cos(2\pi f_x U\tau)\right]$$

When we recall that for $\bar{V} = Ua_x$ then the burst rate parameter becomes from equation B.15

$$R = U\rho A_v \qquad (B.27)$$

where ρ was the scatterer number density and A_v is the crossectional area used to find $p_\lambda(\lambda)$. Thus we see that while the velocity U remains in the shape of $\langle \lambda(t)\lambda(t+\tau)\rangle$, it cancels in the amplitude multipliers. If we note that in B.25

$$N = \frac{T}{\Delta\tau} \qquad (B.28)$$

where T is the total data collection time, the result of combining equation B.25 - B.28 is

$$\langle A_j \rangle = T\Delta\tau\left(\lambda_b + \langle \lambda_j \rangle \rho A_v w_o \sqrt{\frac{\pi}{2}}\right)^2$$

$$+ \frac{\langle \lambda_j^2 \rangle T\Delta\tau\rho A_v w_o \sqrt{\pi}}{2} e^{-\tau^2 U^2/w_o^2}\left[1 + \frac{1}{2}\cos(2\pi f_x U\tau)\right]$$

This result is related to fundamental system parameters through $p_\lambda(\lambda)$ by the equations

---

*This assumes that the pedastal and AC signal are non-overlapping spectrally so that cross-correlation terms between pedastal and AC portions vanish. It also neglects the behavior in the vicinity of $\tau = o$ ($\tau_h << \Delta\tau$).

$$\langle \lambda_j \rangle = \int_{-\infty}^{\infty} \lambda p_\lambda(\lambda) d\lambda \qquad (B.30)$$

and

$$\langle \lambda_j^2 \rangle = \int_{-\infty}^{\infty} \lambda^2 p_\lambda(\lambda) d\lambda \qquad (B.31)$$

B.2.2 Source Distribution

In equation B.29 we used the simple definition of burst rate given by equation 3.15 and avoided the complexities of Section B.1.3.3. Generally speaking, the function $p_\lambda(\lambda)$ has no useful definition independent of A_v; likewise, ρ is an ambiguous term because there may be large numbers of scatterers too small to contribute significantly to the accumulator output. The significant quantity in B.29 is the limit function $\xi(\lambda)$ defined by

$$\xi(\lambda) = \lim_{\substack{A_v \to \infty \\ a_1 \to 0}} \frac{r_\lambda(\lambda, a_1, \bar{A})}{U} \qquad (B.32)$$

where equation B.22 and B.23 are used with $|\bar{V}(t)| = U$. When equation B.32 is substituted in B.29 with the identification of $W_x = w_o\sqrt{\pi/2}$ as the effective probe width in the direction of flow we obtain

$$\langle A_j \rangle = T\Delta\tau\left[(\lambda_b + W_x \int_o^{\infty} \lambda\xi(\lambda)d\lambda)^2 + \frac{W_x}{\sqrt{2}} \int_o^{\infty} \lambda^2 \xi(\lambda)d\lambda \cdot \underset{\text{function}}{\text{shape}}\right] \qquad (B.33)$$

Equation B.33 applies to the result of using a real-time digital correlator with full multiplication. In the dual-

correlate and subtract system we are to construct, only a portion of the right hand integral form in B.33 remains in the accumulator result; but the constant term contributes to the statistical variance of the result. The quantity which determine the weighting of the result according to the amplitudes λ_j and their relative number is $\lambda^2\xi(\lambda)$. This weighting function is well behaved even if $\xi(\lambda)$ has a first or second order pole at $\lambda = 0$, and if $\xi(\lambda)$ becomes monotonically decreasing faster than λ^{-3} beyond some value of λ.

If the product $\lambda^2\xi(\lambda)$ is still significant at values of λ where single photoelectron pulse overlap or discriminator dead time effects begin to dominate, then these effects will truncate the weighting factor for the larger volumes of λ. If $\xi(\lambda)$ is not decreasing faster than λ^{-2} at this point the maximum of the truncated weighting function will occur at the point where nonlinear saturation effects set in. We have no idea at this time what the effect of this region will be on the output.

B.2.3 Example: Monosized Scatterers

The use of the notation $\xi(\lambda)$ simplifies notation while obscuring the communication. As an enlightening example we return to the case 2 optical system with monosized scatterers. In that case the use of ρ for number density was not ambiguous, and A_v can be conditionally defined as

$$A_v = 2cw_oL_z \ . \qquad \text{(B.34)}$$

when this is done, equation B.11 gives the conditional density $p_\lambda(\lambda|c)$ and we have

$$\lambda^2 \xi(\lambda) = \lambda^2 \lim_{c \to \infty} \rho(2cw_o L_z) p_\lambda(\lambda|c) \qquad (B.35)$$

$$= \frac{w_o L_z \rho \lambda}{\sqrt{2}\sqrt{-\ln(\frac{\lambda}{\gamma_o})}} \quad 0 < \lambda < \gamma_o$$

where γ_o is the peak value of λ_j for particles through the center of the probe volume. The definition of $\xi(\lambda)$ avoids the anomalies which arise in the definition of $p_\lambda(\lambda)$ due to probe volume boundaries which are not well defined. The λ^2 multiplier (or the λ multiplier in determining the constant part of $\langle A_j \rangle$) removes the singularity at $\lambda = 0$. The function $\lambda/\sqrt{-\ln(\lambda/\gamma_o)}$ is plotted in Figure B2 for $\gamma_o = 1$.

B.2.4 Interpretation for Particle Size Distribution

If we recall equation .6a and insert this in the definition of the weighting factor $\lambda^2\xi(\lambda)$ we see that the λ^2 term may be carried inside the integral with the result:

$$\lambda^2 \xi(\lambda) = \lim_{A_v \to \infty} \int_{-\infty}^{\infty} p_\gamma(\alpha) \left[\frac{\rho A_v \lambda^2}{|\alpha|} p_\gamma(\frac{\lambda}{\alpha} |A_v) \right] d\alpha \qquad (B.36)$$

We recognize this as a superposition integral with the term in brackets being the weighting function for a single particle size which produces a value of $\gamma = \alpha$. The integral adds these functions with weighting by the density for γ.

We have finally reached the point where we can determine the composition of the photon correlator accumulator result in terms of particle size. To do this we reinsert $\lambda^2\xi(\lambda)$ from equation B.36 into equation B.33 and interchange the order of integration. Integrating with respect to λ first leaves the second term in B.33 as

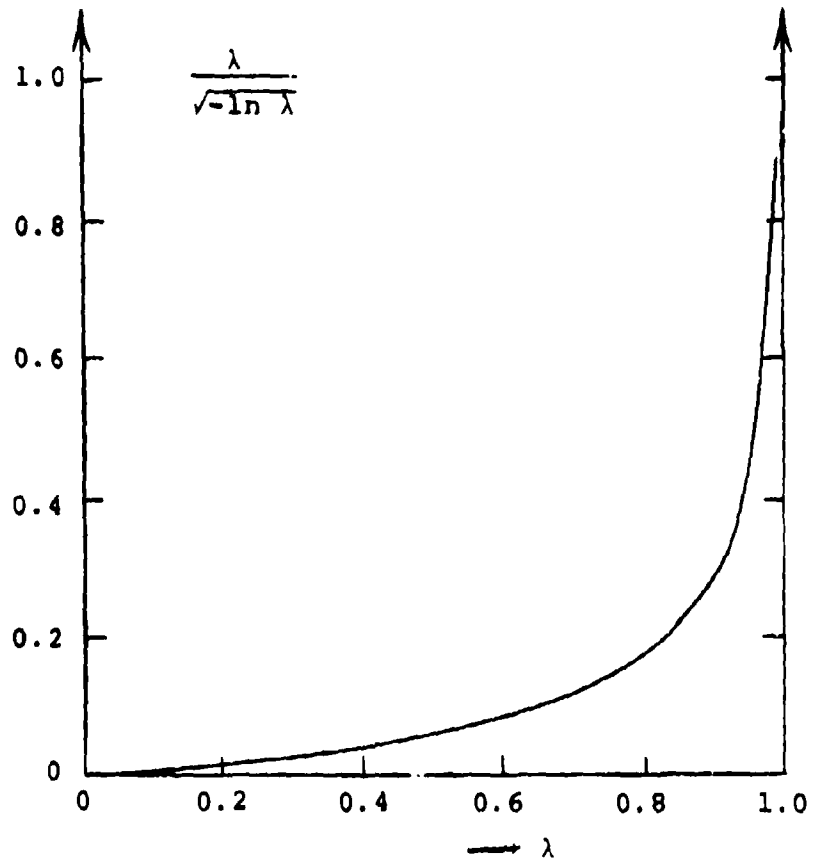

Figure B2. Photon Correlation Signal Weighting Function Shape for Monosized Scatterers.

$$\frac{W_x}{\sqrt{2}} \int_{-\infty}^{\infty} p_\gamma(\alpha) \left[\lim_{A_V \to \infty} \int_0^{\infty} \frac{\rho A_V \lambda^2}{|\alpha|} p_\gamma\left(\frac{\lambda}{\alpha} | A_V\right) d\lambda \right] d\alpha \qquad (B.37)$$

A similar expression with λ instead of λ^2 holds for the first term in B.33. The result of the inner integral in equation B.37 is a function of the dummy integration variable α which represents γ. The variable γ is directly related to particle size through the Mie scattering law.

The theory which relates the particle size distribution to the photon correlator accumulator outputs is more complex than we originally believed. We have obtained results theoretically, but at the present we have not had time to extend the generality beyond a specific somewhat simplified optical model or to evaluate the integrals parametrically to obtain more graphic results.

B.3 APPLICATION TO BURST COUNTER SYSTEM

The objectives of the first extension of our present contract included development of a statistical signal model that would benefit both the development of photon correlation and the further refinement of burst-counter systems. We can not go much beyond opening the door with respect to burst-counter applications because of scope limitations; but we would like to briefly indicate the nature of several tentative conclusions we have drawn without having had time to pursue very detailed analytical or computational studies.

B.3.1 Transient Filter Response-SNR

We have experimentally observed filtered low-level LV signals which not only demonstrated the non-stationary and signal-dependent nature of the noise but also exhibited a time-delay shift of the high-frequency portions of the noise

with respect to the signal waveform. In this observation, the positive-going zero-crossing portions of the signal appeared to be much less noisy than the negative-going zero-crossing portions. In this instance it was significant that the signal polarity was chosen to count fringe periods on the positive-going zero-crossings and not the negative-going zero-crossings.

When Gaussian noise is filtered by a linear filter, only the magnitude of the frequency transfer function for the filter is significant for the output noise of the filter. This is true because the statistics of the output noise are completely determined by the output power spectrum which is the product of the input power spectrum and the magnitude square of the Fourier transform of the filter impulse response. The experimental observation mentioned in the above paragraph and the theory of Section 2 show that the time distribution of the noise with respect to the signal is affected by the transient response of the filter (or its entire Fourier description, including the phase characteristic.) This matter should be pursued further in the future.

B.3.2 Detection Improvement

In a burst-counter the functions of detecting the presence of a burst, estimating the mean period, and deciding whether the data word is acceptable are three separate functions. With state-of-the art error rejection (decision) circuits, valid data can be obtained by setting the detection threshold low and rejecting invalidated data. However, information is lost where the threshold detection circuit triggers on a noise fluctuation and the estimation dead time causes the system to miss a burst which would have produced a validated measurement.

There are two simple ways to significantly improve the threshold detection efficiency of a burst-counter. The first is to use state-of-the art PMT's to minimize probability of occurrences of anomalously large single-photo-electron pulses. The second is to provide a separate signal path and filter for the threshold detection and the period estimation circuits. To be specific, if the optical system restricts the field of view of the PMT so that all or almost all pedastal signals are accompanied by a sinusoidal signal-burst component, then a good detection filter is a low-pass pedastal detection filter with much less bandwidth than is required for the period estimation circuits.

B.3.3 Particle Size Effects

For a given LV system and set of measurement parameters we have the following composition for the output validated data rate:

$$R_{vd} = \int_0^\infty r_\lambda(\lambda) P_{gd}(\lambda) d\lambda + R_{\varepsilon d} P_{v\varepsilon d} \qquad (B.38)$$

where $r_\lambda(\lambda)$ is the burst rate amplitude distribution described in Section B.1, $P_{gd}(\lambda)$ is the probability that a burst of amplitude $\lambda_j = \lambda$ will be detected and produce a validated estimate, $R_{\varepsilon d}$ is the rate at which the processor triggers on background fluctuations (estimation produces erroneous and irrelevant data), and $P_{v\varepsilon d}$ is the probability that validation occurs with a false trigger. The quantities P_{gd}, $R_{\varepsilon d}$, and $P_{v\varepsilon d}$ are

functions of the background light level, the detection threshold, the processor dead time and the total burst rate (things get much more complicated when the probability is appreciable that the detection threshold will be crossed more than once during the processor dead time; also if there are subthreshold bursts present during a detected burst, the noise and interference are higher and $P_{gd}(\lambda)$ is lower.) Generally, the problem we wish to solve is the maximization of the good data rate with constraints on $R_{\varepsilon d}$, $P_{v\varepsilon d}$ and with other constraints (such as no seeding, a certain system cost, a minimum acceptable data rate, etc.) The statistical signal model we have presented above with generalization of the optical model and proper modeling of the flow/particle dynamics and the processor components form the basis for constructing a system optimization code which could be used in measurement planning or on-line system optimization.

The complexity of equation B.38 is considerable when all the dependence of the many deterministic and random system parameters are shown explicitly. Some of the contract time was devoted to attempts at being more specific and obtaining a very crude model for $P_{gd}(\lambda)$ so that there would be some quantitative comparison between the source distribution for photon correlation output and burst counter output. The task was quite beyond the limitations of time under which we were working. The significant thing we have done in this area is establish a common approach for the comparison and optimization of LV processors. The basis is in the function $r_{\lambda}(\lambda)$ (or the related $\xi(\lambda)$) and the composition of this function in terms of the particle size distribution and the random probe volume multiplier effects.

B.4 MEASUREMENT AND SCALING OF RATE/AMPLITUDE FUNCTIONS

We have shown that measurement time (or data rates) for photon correlation (or burst counters) depend on an integral superposition of $\xi(\lambda)$ (or $r_\lambda(\lambda)$) which has been related to particle size number density and optical parameters. In this section we consider the two separate problems of experimental measurement of this function and its scaling behavior with changes in system parameters. These two problems are related because the quantity $\lambda(t)$ and the separate burst amplitudes λ_j are not always directly measurable, and scaling may be essential.

B.4.1 Direct Measurement

The measurement of $\lambda(t)$ exactly is not possible. The trade-off is, as usual, between resolution (bias error) and noise (statistical variation). Equation 2.7 may be rewritten as

$$\langle i(t) \rangle = e \langle g_i \rangle \lambda(t) \tag{B.39}$$

when h(t) is a low-pass pulse and, τ_h is small enough for h(t) to behave as an impulse function with respect to the time variation of $\lambda(t)$. Under the same condition equation 2.8 becomes approximately

$$\sigma_i^2(t) = \frac{e^2}{\tau_h} \langle g_i^2 \rangle \lambda(t) \tag{B.40}$$

and the instantaneous fractional rms deviation is

$$\frac{\sigma_i(t)}{\langle i(t) \rangle} = \frac{\sqrt{\langle g_i^2 \rangle}}{\langle g_i \rangle} \frac{1}{\sqrt{\lambda(t)\tau_h}} \tag{B.41}$$

Thus, if $\lambda(t)\tau_h >> 1$, i(t) is proportional to $\lambda(t)$ with small variation. If this condition were valid for the LV signals of interest we wouldn't be concerned with any of the present effort.

Fortunately, for "sparse" bursts,* the requirements for measurement of the distribution of burst amplitudes λ_j are not as stringent as those for continuous estimation of $\lambda(t)$. We will only consider a simple sub-optimal approach since the optimal measurement of $\xi_\lambda(\lambda)$ could be the subject of a study in itself. If a low-pass filter is used which passes the burst pedastal but not the sinusoidal signal, then the value of τ_h in B.40 is increased, the convolution in 2.8 removes the sinusoidal portion of $\lambda(t)$, and we would replace $\lambda(t)$ in B.41 with $\lambda_p(t)$, the pedastals only. From equation B.3 we note that this leaves λ_j as the peak value of a Gaussian pulse at the point where the fractional rms deviation B.41 is minimum. Due to the increase in τ_h obtained by reducing the filter bandwidth, smaller values of λ_j can be measured than if a peak detector were applied to the direct output of the photomultiplier tube.

In order to extend the measurement to smaller values of λ_j there are several straight-forward improvements of the

*The phrase "an average of less than one scatterer in the probe volume" is very ambiguous here. What is usually implied in the LV literature is that for the detection threshold and filter which are being used, the average burst separation is much greater than the burst duration. A typical probe volume for high velocity air flow measurements can easily contain an average of more than one scatterer if all the smaller scatterers are counted. With typical filter bandwidths for transonic measurements, the bursts produced by the smaller scatterers are photon resolved; thus the appearance of the signal is that of "sparse" bursts plus background when in fact some of the "background" is low-level overlapping or non over-lapping signals.

above procedure. The first is to reduce the air velocity to a very small value and thereby reduce the required bandwidth and extend τ_h. In this manner values of λ_j may be measured by a peak detector even though the same scatterer size will produce photon-resolved signals at higher velocities (with wider bandwidth filters). We have used this method in the experimental work reported in the section 5.0.

For on-line measurements at high velocity or for situations where the particle number density is too large for the "sparse" condition to be valid another approach would be to expand the laser beams incident on the transmitting lens and reduce the collecting system spatial filter aperture. This would increase the incident optical power density by the square of the expansion while increasing the filter bandwidth required only linearly. The scaling laws of the next section could then be applied.

Additional improvement of the above approaches would result from reducing the bandwidth further by replacing the filter with an integrator and logic which measured the step level change (total burst energy) and then reset the integrator to zero before the next burst occurred. An integrating particle size instrument has recently been developed by M. Farmer, J. Hornkold, et. al. at SAI Tullahoma. A modification of that instrument or similar integrating circuitry could be useful in later efforts along these lines.

All of the above methods become unreliable at levels so low that background fluctuations are detected as signal bursts, and further study of the statistical estimation of $\xi_\lambda(\lambda)$ by photon counting methods may later be appropriate.

B.4.2 Scaling

The scaling laws are implicit in the theory, but are stated here for convenience. With the exception of velocity

effects (since $r_\lambda(\lambda) = |\bar{V}|\xi_\lambda(\lambda)$) the functions $r_\lambda(\lambda)$, and $\xi_\lambda(\lambda)$) scale the same way so we refer only to $r_\lambda(\lambda)$ and its integral $R_\lambda(\lambda > \lambda_1)$.

B.4.2.1 Velocity

$\xi_\lambda(\lambda)$ is not affected but our ability to measure the function is affected. $r_\lambda(\lambda)$ and $R_\lambda(\lambda > \lambda_1)$ are proportional to velocity unless velocity change also changes the size/number density distribution of scatters in the air (such as the occurrence of condensation during a wind tunnel test).

B.4.2.2 Effective Collected Power

An increase in collected effective power (laser power, PMT quantum-collection efficiency, optical transmission efficiency, collecting* f/no) by a factor k will produce $r'_\lambda(\lambda)$ given by

$$r'_\lambda(\lambda) = \frac{1}{k} r_\lambda(\lambda/k) \tag{B.42}$$

The 1/k multiplier does not enter in the integral quantities, i.e.:

$$r_\lambda(\lambda > \lambda_1) = R_\lambda(\lambda > \frac{\lambda_1}{k}) \tag{B.43}$$

This is important since the cumulative function may be measured and differentiated to obtain the differential function.

B.4.2.3 Incident Beam Diameter

An increase in the waist diameter of the parallel beams incident on the transmitting lens by a factor of k with corresponding reduction by a factor k of the probe diameter

*Simplistic model for small scatterers not considering scatter lobe patterns.

w_o, and all dimensions of the collecting system spatial filter aperture, changes the shape (number of fringes of the burst) and effects the distribution functions as

$$r'_\lambda(\lambda) = \frac{1}{k^4} r_\lambda \left(\frac{\lambda}{k^2}\right)$$

$$R'_\lambda(\lambda > \lambda_1) = \frac{1}{k^2} R\left(\lambda > \frac{\lambda_1}{k^2}\right)$$

In this instance the distribution expands to the higher values of λ as k^2 because of the square increase in incident intensity. There is an additional $1/k^2$ factor due to the square decrease in probe-volume cross-section area. We should also point out that for a photon correlation system this change also reduces the value of W_x in equation B.33 by $1/k$.

Comment: If the collection optics spatial filter aperture is not scaled along with the probe volume beam diameter, the shape of $r_\lambda(\lambda)$ is changed so that no simple scaling is possible.

B.4.2.4 Transmitter Focal Length

If the transmitter focal length is reduced by a factor k, and the collecting optics spatial filter is reduced in each dimension by k, and the scattering angle is not changed (off axis collecting lens moved closer to transmitting lens with smaller diameter but same f/no.) The effects are essentially the same for the λ_j distributions as above in B.4.2.3. (However, the fringe number remains the same so system bandwidth increases).

B.4.2.5 Wavelength

It would be very helpful if we could measure $r_\lambda(\lambda)$ at one wavelength and determine by scaling what the effects of

switching to a laser of a different wavelength would be. If all the scatterers of interest were much less than the optical wavelength in diameter, this could be done because the scattering intensity from all Rayleigh sized scatterers is proportional to λ^4 (the product of $i(a)\lambda_o^2$ is proportional to λ_o^4 in equation B.2). The scaling would have to include a change in w_o as well as all the other dependent factors in equation B.2. In all applications of interest that seem relevant, however, the submicron and even larger Mie scatterers contribute significantly and the distributions are not scalable.

B.4.2.6 Optical Geometry Changes

Due to the complexity of the probe volume geometry effects and the Mie scattering functions, most changes in the optical system such as polarization, scattering angle, spatial filter size or shape, etc. do not produce scalable changes in the distribution functions. This means that a thorough parametric study of the behavior of the functions we have been describing will require extensive computer calculations or experimental measurements. Our experiments have demonstrated that the power law behavior of the distributions of λ is significantly affected by the optical system parameters.

LIST OF SYMBOLS

ENGLISH

a	particle radius
a_j	PMT anode voltage at pedastal peak; particle radius (in Appendix B)
A_j	accumulator value at $\tau = j\Delta\tau$
B	bandwidth
c	spatial filter aperture width = $2cw_o$
$C_{ii}(t_1,t_2)$	autocovariance of $i(t)$
D	diameter of collecting objective
e	electronic charge
$f(\ )$	optical probe volume response function
F	focal length of collecting objective; PMT collection efficiency
g_i	random single-photoelectron charge gain
h	Planck's constant
$h(t)$	impulse response of PMT and succeeding filters
$H(\omega)$	Fourier transform of $h(t)$
i	counting index
$i(t)$	photocurrent at anode or succeeding filter output
I	optical intensity
j	counting index
k	counting index, or arbitrary constant in scaling
L_z	probe volume length
$m_i(t)$	time varying statistical mean current $\langle i(t) \rangle$
m_k	$n_k n_{k-p} - n_k n_{k-q}$ or other function of n_k
$\hat{M}_p$	photon correlation sum at delay $p\Delta\tau$
$\hat{M}_{pq}$	accumulation at $(p\Delta\tau, q\Delta\tau)$ for Dual Correlate Mode
$n(t_1,t_2)$	photoelectron count in interval (t_1,t_2)
$n_a(a)$	differential particle number density
n_k	photon count in $\Delta\tau$ interval about $k\Delta\tau$
N	number of time increments $\Delta\tau$ $(T = N\Delta\tau)$
$N_a(a > a_1)$	number of particles with radius $a > a_1$ per unit volume: $N_a(a > a_1) = \int_{a_1}^{\infty} n_a(a)da$

$p_x(x)$	probability density for random variable x
$p_x(x\|y,z)$	conditional probability density for x given the values of the random variables y and z
$P\{A\}$	probability of the event A
$P_x(x > x_1)$	probability that the random variable x exceeds the value x_1
$P(t)$	optical power incident on photocathode
q	integer value of delay; power law a^q, q real
r	power law a^r
$\bar{r}_j$	random translational location of jth particle WRT probe center
$r_\lambda(t,\lambda)$	differential amplitude burst rate
$R(t)$	instantaneous rate of signal bursts
$R_\lambda(t,\lambda>\lambda')$	mean rate of bursts at time t with λ_j > the value λ' given by $\int_{\lambda'}^{\infty} r_\lambda(\lambda)d\lambda$ (in Appendix only)
$R_\lambda(\tau)$	autocorrelation of $\lambda(t) = \langle\lambda(t)\lambda(t+\tau)\rangle$
$s(t)$	a generalized Poisson shot noise signal (Appendix A)
t	time
T	total data collection time
T_m	inverse of mean burst frequency
$u(t)$	time varying velocity component
$U(t)$	total velocity component
U	mean velocity component
$\bar{V}$	vector velocity
w_o	$1/e^2$ intensity radius at beam waist
W_x	effective probe volume width in direction of flow
x	position variable
y	position variable
y_j	random y displacement of jth particle from probe center
Y_j	random probe volume amplitude multiplier due to y_j
z	position variable
$z(t)$	Poisson impulse process

GREEK

α	integration dummy variable; also 1/e half-width of burst
β	integration dummy variable
$\delta(t)$	Dirac delta or unit impulse function
γ_j	peak value λ_j which would result if particle went through the probe volume center
ε	rms error
$\lambda(t)$	time varying mean rate of photoelectron pulses $\lambda(t) = \eta P(t)/h\nu$
λ_b	steady background photoelectron rate
λ_j	peak photoelectron rate (pedastal) from the jth scatterer. $\lambda_j = \gamma_j Y_j$
λ_o	optical wavelength
λ_s	mean signal photoelectron rate $\neq \langle\lambda_j\rangle$ (see equation 3.24)
η	product of photocathode quantum efficiency and dynode collection efficiency
ν	optical frequency
$\sigma_i^2(t)$	time varying variance of i(t): $\langle(i(t)-\langle i(t)\rangle)^2\rangle$
τ	delay variable
τ_h	rise time or pulse width of low pass h(t)
τ_j	occurrence time for jth signal burst
θ	beam intersection angle; spherical declination angle from direction of incident light
ϕ	polar angle
μ	Poisson parameter
ω	Fourier transform variable or radian frequency
ω_j	random frequency of jth burst
ω_m	mean of random variable ω_j
$\xi_\lambda(\lambda)$	normalized differential rate function $r_\lambda(\lambda)/\lvert\bar{V}\rvert$

Special Notation

$\langle x\rangle$	statistical expectation of $x = \int_{-\infty}^{\infty} x\, p_x(x)dx$
$f(t)*g(t)$	convolution: $\int_{-\infty}^{\infty} f(\alpha)g(t-\alpha)d\alpha$